SPECTRAL ANALYSIS OF PARABOLIC RANGE GATE PULL-OFF SIGNALS IN DIGITAL RADIO FREQUENCY MEMORY

A MASTER'S THESIS

in

Electrical and Electronics Engineering

Atilim University

by

MUSTAFA TALHA ÖZTÜRK

JANUARY 2015

SPECTRAL ANALYSIS OF PARABOLIC RANGE GATE PULL-OFF SIGNALS IN DIGITAL RADIO FREQUENCY MEMORY

A THESIS SUBMITTED TO

THE GRADUATE SCHOOL OF NATURAL AND APPLIED SCIENCES

OF

ATILIM UNIVERSITY

BY

MUSTAFA TALHA ÖZTÜRK

IN PARTIAL FULFILLMENT OF THE REQUIREMENTS FOR THE DEGREE OF

MASTER OF SCIENCE

IN

THE DEPARTMENT OF ELECTRICAL ELECTRONICS ENGINEERING

JANUARY 2015

Approval of the Graduate School of Natural and Applied Sciences, Atılım University.

_____

Prof. Dr. İbrahim AKMAN

Director

I certify that this thesis satisfies all the requirements as a thesis for the degree of Master of Science.

_____

Assoc. Prof. Dr. Elif AYDIN

Head of Department

This is to certify that we have read the thesis "Spectral Analysis Of Parabolic Range Gate Pull-Off Signals in Digital Radio Frequency Memory" submitted by "Mustafa Talha ÖZTÜRK" and that in our opinion it is fully adequate, in scope and quality, as a thesis for the degree of Master of Science.

_____

Assoc. Prof. Dr. Ali KARA

Supervisor

Examining Committee Members

Doç. Dr. Ali KARA _____

Yrd. Doç.Dr. Ahmet PAKFİLİZ _____

Yrd. Doç. Dr. İ. Baran USLU _____

Yrd. Doç. Dr. H. Taha HAYVACI _____

Dr. İbrahim ÖZ _____

Date: (30.01.2015)

I declare and guarantee that all data, knowledge and information in this document has been obtained, processed and presented in accordance with academic rules and ethical conduct. Based on these rules and conduct, I have fully cited and referenced all material and results that are not original to this work.

Mustafa Talha ÖZTÜRK

Signature:

ABSTRACT

SPECTRAL ANALYSIS OF PARABOLIC RANGE GATE PULL-OFF SIGNALS IN DIGITAL RADIO FREQUENCY MEMORY

ÖZTÜRK, Mustafa Talha

M.S., Electrical Electronics Engineering Department

Supervisor: Assoc. Prof. Dr. Ali KARA

January 2015, 57 pages

Digital Radio Frequency Memory (DRFM) is a device that is used in electronic warfare area to apply electronic attack techniques and manipulate the enemy's radar signals by copying the received radar signals. Range Gate Pull-Off (RGPO) technique which is used with DRFM is one of the key electronic attack (EA) techniques, and it can be applied as linear or parabolic RGPO according to the applied pull-off function. This thesis study includes the signal derivation of DRFM linear RGPO signal which is presented in the literature, and based on this it includes realized DRFM parabolic RGPO signal derivation. Also, this work presents the linear and parabolic RGPO scenarios which generated different DRFM and RGPO parameters, and spectrum results and analysis of these scenarios.

Keywords: Digital Radio Frequency Memory, DRFM, Range Gate Pull-Off, Linear RGPO, Parabolic RGPO

ÖZ

DİJİTAL RADYO FREKANS HAFIZASI PARABOLİK MESAFE KAPISI KAYDIRMA SİNYALLERİNİN SPEKTRAL ANALİZİ

ÖZTÜRK, Mustafa Talha

Yüksek Lisans, Elektrik Elektronik Mühendisliği Bölümü

Tez Yöneticisi: Doç. Dr. Ali KARA

Ocak 2015, 57 sayfa

Dijital Radyo Frekans Hafızası (DRFM), alınan radar sinyallerini kopyalayarak elektronik taarruz teknikleri uygulamak için ve düşman radar sinyallerini manipüle etmek için elektronik harp alanında kullanılan bir cihazdır. Bu cihaz ile kullanılan temel elektronik taarruz tekniklerinden birisi de mesafe kapısı kaydırma (RGPO) tekniğidir ve bu teknik uygulanan geciktirme fonksiyonuna göre lineer veya parabolik olarak uygulanabilmektedir. Bu çalışma, literatürde bulunan DRFM lineer RGPO sinyal türetimlerini ve bu analizden yola çıkılarak gerçekleştirilen parabolik RGPO sinyal türetimlerini içermektedir. Ayrıca lineer ve parabolik RGPO teknikleri için farklı DRFM ve RGPO parametreleri ile oluşturulmuş senaryoları ve senaryolara ait spektrum sonuçlarını ve analizlerini sunmaktadır.

Anahtar Kelimeler: Dijital Radyo Frekans Hafızası, Lineer Menzil Kapısı Çalma, Parabolik Menzil Kapısı Çalma

To My Parents

ACKNOWLEDGEMENTS

I express sincere appreciation to my supervisor Assoc. Prof. Dr. Ali KARA for his advice, criticism, guidance and insight throughout the research.

I would like to thank my whole family; for their care on me from the beginning of my life, their prayers, and their trust on me that I could accomplish this task.

TABLE OF CONTENTS

LIST OF TABLES

TABLE

LIST OF FIGURES

FIGURES

LIST OF ABBREVIATIONS

ADC	-	Analog-to-Digital Converter
AGC	-	Automatic Gain Control
ARM	-	Anti Radiation Missile
CPI	-	Coherent Pulse Interval
CW	-	Continuous Wave
DAC	-	Digital-to-Analog Converter
DRFM	-	Digital Radio Frequency Memory
EA	-	Electronic Attack
ECM	-	Electronic Countermeasures
ECCM	-	Electronic Counter Countermeasures
EP	-	Electronic Protection
ES	-	Electronic Support
ESM	-	Electronic Support Measures
EW	-	Electronic Warfare
FFT	-	Fast Fourier Transform
FML	-	Frequency Memory Loop
IR	-	Infrared
LO	-	Local Oscillator
MTI	-	Moving Target Indicator
PD	-	Pulse Doppler
PPI	-	Plan Position Indicator
PRF	-	Pulse Repetition Frequency

PRI	-	Pulse Repetition Interval
RF	-	Radio Frequency
RFT	-	Range False Target
RGPO	-	Range Gate Pull-Off
RGPI	-	Range Gate Pull-In
RWR	-	Radar Warning Receiver
SPP	-	Stationary Phase Principle
TOA	-	Time of Arrival
VFT	-	Velocity False Target
VGPO	-	Velocity Gate Pull-Off
VGPI	-	Velocity Gate Pull-In

CHAPTER 1

INTRODUCTION

Electronic Warfare (EW) is described to control and exploit electromagnetic spectrum which contains radio frequency (RF), infra-red (IR), visible and ultraviolet bands or to attack the enemy in a warfare environment in the name of homeland security and defense [1],[2]. EW includes three major subdivisions: electronic support (ES) or electronic support measures (ESM), electronic protection (EP) or electronic counter-countermeasures (ECCM) and electronic attack (EA) or electronic countermeasures (ECM).

ES is a division of EW which includes actions taken for searching, intercepting, localization, recording and analyzing radiated signals, for the purpose of using these radiations to support military operations [1],[2]. Thus, ES is an important source of information to perform EA and EP operations which are other branches of EW.

EP is another branch of EW which includes actions taken for protecting crews, equipment and plants from any effects of electromagnetic radiations which can belong to enemy forces which can degrade, neutralize, or destroy friendly combat capability [2]. Shortly, EP could be described as strength to jamming or EA sources.

EA interests in the use of electromagnetic spectrum or directed power to attack the hostile's combat forces directly. EA branch combines the hard kill which contains the operations to degrade enemy weapons with the destruction ability of anti-radiation missiles (ARMs) and directed energy weapons, and soft kill which contains the operations of jamming and deception actions to make ineffective the enemy electromagnetic radiation or radio frequency sources. Jamming actions is described as radiation or reflection of electromagnetic energy to suspend the enemy's use of electromagnetic spectrum. On the other hand, deception actions are described as radiation, suppression, absorption or reflection of electromagnetic energy to mislead

the enemy's information sources or to prevent the use of information by enemy sources [1]. Noise jamming techniques like spot noise, barrage noise, etc. as jamming actions, and false target techniques like range and velocity false target (RFT and VFT), range gate pull-off (RGPO), velocity gate pull-off (VGPO), etc. as deception actions can be applied with on-board active EA devices. Digital Radio Frequency Memory (DRFM) which is the topic of this thesis work, Frequency Memory Loop (FML) and other repeater systems place in the active on-board EA systems under deception jammers title as repeater jammer devices.

In EW environment, the first step is detecting the electromagnetic radiations to develop any countermeasures or attack signal. So, EW applications start with recognizing the radar and weapon system of the enemy forces. Radar Warning Receivers (RWR) is first designed EW system in history. After development of RWRs, countermeasure system is designed to neutralize the recognized target. Jamming techniques are developed to prevent recognizing by enemy radar system. After jamming signals are distinguished by radars, FML, which has the ability of transmitting the received radar signal with time delay, has been started to use in EW environments. After a while, FMLs fall behind because of the developments in radar technology and EP techniques. Thus EA applications switch to DRFM technology that has already being developed today for more effective techniques. [4].

DRFM is an EA device used to store threats' radar signals in a digital memory unit with high speed sampling. These stored data allow for deceiving threat radar system by transmitting the deceptive radar signal after copying and changing some parameters of the stored signal. The most important advantage of DRFMs is capability of deceiving radars that check coherency of the received signal. A radar system, which controls coherency, can recognize difference between its echo and signal comes from a repeater device like FML, because of the non-coherent EA signal. Hence, such a radar system can change its mode or use EP capabilities after detection of the EA signal to discard effects of the EA signal, and in this point DRFM system overrides to other repeater hardware systems since it produces deceptive EA signal copying the threat radar signal one-to-one and without phase distortion from pulse to pulse [4],[5].

In the open literature, previous researches on DRFM have generally focused on the harmonics or spurs due to the discrete nature of the analog-to-digital converter (ADC). Berger and Meer [6], Roome [7] and Kernis [8] ensure that the results on spacing and magnitude of the spurs which are related with the harmonics of the sampling rate and number of bits are used in quantization caused by the ADC unit of DRFM hardware. Gold and Ur [9] serve a method to reduce spurs produced by ADC by introducing a random timing jitter. The spurious signals caused by the discrete nature of the ADCs can be used to detect the existence of a DRFM deception by radar or EP systems, so Hill and Truffert [10] present an analysis of a DRFM detection proposal which is based upon the quantization noise detection. At the systems level, Dunn-Rogers [11] analyzes the effect of I and Q channel imbalance on DRFM performance, and Pring et. al. [12] represents a phase performance analysis of DRFMs. As a different analysis from ADC, Blair and Brandt-Pearce [13] suggest and analyze a method for discrimination between target pulses and DRFM range gate pull-off pulses. This approach is based on a statistical analysis about fluctuations on amplitude for the DRFM pulses and target pulses. In another study, Berger [14] analyzes the spectrum of the DRFM linear RGPO signal using discrete time delay resolution, update period and pull-off rate parameters. In this study, an analysis is presented to predict spectral characteristics of the DRFM linear RGPO signal, but it does not include magnitude of these spectral harmonics. After that, Berger [15] represents an analytical expression for the frequency spectrum of a DRFM linear RGPO signal that reveals the magnitude of the spectral harmonics. Badiera, Rarina, Orlando and Ricci [16] in their study address detection algorithm to discriminate between the generated target signal by a DRFM system and backscattered real target return signal in thermal noise and clutter existing environment. As a different point of view in the literature recent studies show that the DRFM is also used to test and evaluate radar system in test environments. In this sense, Oliver, Cilliers and Plessis [17] discuss wideband DRFM design and performance criteria for a pulse Doppler radar testing in a hardware-in-the-loop simulator to create target return. Also, Sward and Reed [18] present a comparison between phase continuous target generators and traditional DRFM based radar target generators for radar test applications. They present the benefit of a phase continuous target generator which is a DRFM architecture based device whose memory unit is a digital signal processor.

In the scope of this thesis, the analytical derivations and simulation results which include DRFM linear and parabolic RGPO signals and their spectrums are represented. Introduced analytical derivations and simulations about linear RGPO contain Berger's linear RGPO study [15] with expanded scenario set. The novel part of this thesis work about DRFM is parabolic RGPO. The novelty of the thesis stems from DRFM parabolic RGPO signal derivation and suggested simulation scenarios which are presented with different device and technique parameters for the sake of clarity. As an important contribution, this study also provides an attentive approach to check the given simulation results and to improve the previous study in [15] with additional DRFM linear RGPO scenarios.

The results represented in this study can be evaluated by signal intelligence engineers since the spectral characteristics of the DRFM linear and parabolic RGPO signals ensure additional information for evaluation or estimating EA systems of threat, also EA engineers can be interested in the results because of the chosen parameter set can change the effectiveness of the RGPO technique on threat radar systems.

The remainder of this work is organized as follows. In Chapter 2, the pulse Doppler (PD) radar signal and its spectrum is derived as the input signal of the DRFM. In Chapter 3, firstly, DRFM linear range gate pull-off (RGPO) signal and then DRFM parabolic RGPO signal are derived mathematically. Also, the frequency spectrums of these signals are derived and the effect of the coherent pulse interval (CPI) is explained. Chapter 4 includes the results of the simulated linear and parabolic RGPO techniques using computer simulation to verify the validity of the derived analysis. Finally in Chapter 5, results and concluding remarks are given about the thesis to draw an outline for all about the study, and some suggestions and future works are given.

CHAPTER 2

PULSE DOPPLER RADAR SIGNAL

Radars that rely on the Doppler effect to improve target detection and tracking using the velocity information are called Doppler radars. Doppler radars can be either continuous wave (CW) or pulsed radars as in Figure 2.1. CW radars simply observe the Doppler shift between the carrier frequency of the return signal from target relative to the transmit signal of radar and it produces velocity information about the target by using this observed Doppler shift. Beside, pulsed systems can determine Doppler shift through measuring the phase change that occurs in a coherent pulse train which stands for continuity in phase for each pulse in the pulse train. Coherency in the pulse train of radar signal concentrates the energy in the spectrum around distinct spectral lines which are separated in frequency spectrum by the pulse repetition frequency (PRF) of the radar and also this separation allows for distinction of Doppler shifts in the echo signal [19]; on the other hand, a pulse train whose phase starts randomly for each pulse is called non-coherent pulse train.

A pulse radar, which uses the Doppler shift to detect moving targets, can be either an MTI (moving target indication) radar or a PD radar. MTI radars have PRF values which are low enough to have no range ambiguities, but they have ambiguities in the Doppler o velocity domain because of the low PRF or, inversely, high PRI values. On the other hand, PD radars have PRF values which are large enough to have no Doppler ambiguities; however they have ambiguities in the range or time domain. Briefly, MTI and PD radars are just the opposite and they have ambiguities in range or Doppler domains. [20].

Theoretically a coherent PD radar signal can be produced by modulating a complex sine wave with a pulsed train or pulsed waveform which comprises uniformly spaced pulses with a constant pulsewidth for infinite time or limited time structure [20].

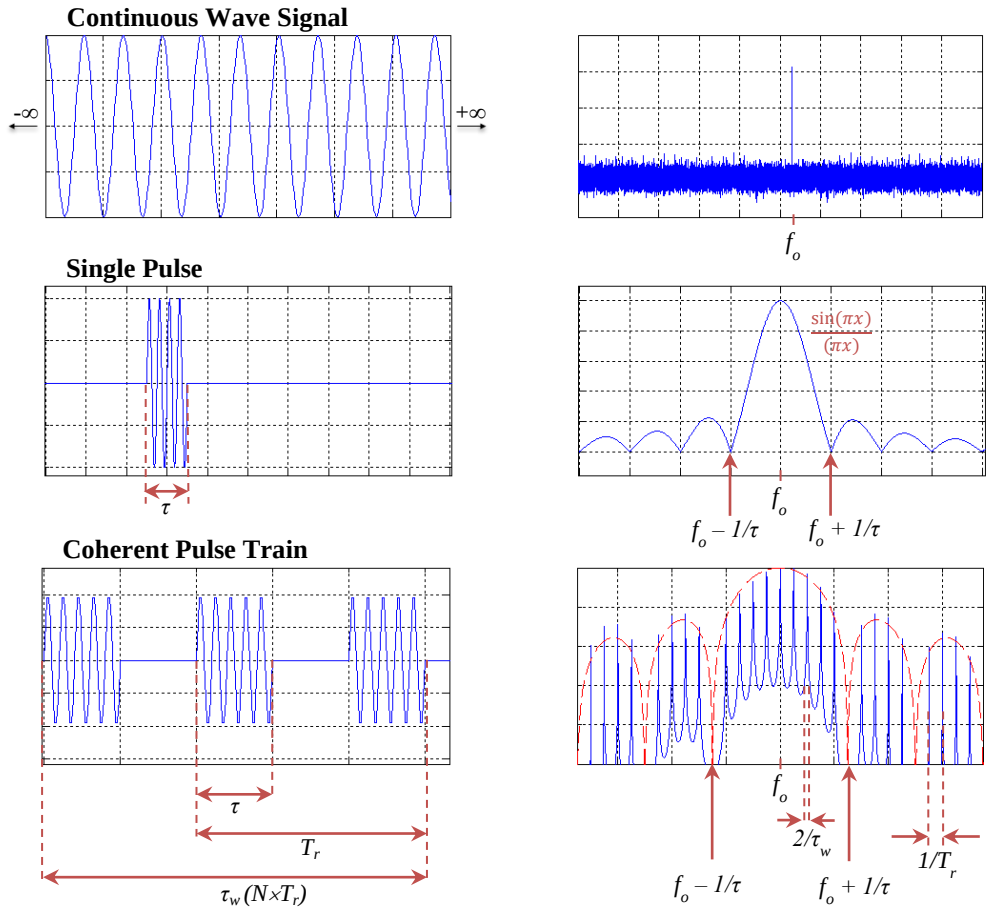

Figure 2.1 CW and Pulsed Radar Signals and Spectrums

The pulsed waveform can be expressed as the equation (2.1) and (2.2) using the infinite time assumption.

$$p_\tau(t) = \begin{cases} 1, & -\tau/2 < t \le \tau/2 \\ 0, & otherwise \end{cases} \tag{2.1}$$

$$p(t) = \sum_{n=-\infty}^{\infty} p_\tau(t - nT_r) = p_\tau(t) * \sum_{n=-\infty}^{\infty} \delta(t - nT_r) \tag{2.2}$$

and spectrum of the pulsed waveform can be written as equation (2.5) using the Fourier transform pairs in equation (2.3) and equation (2.4), and using the fact that convolution of two time domain signal is represented in frequency domain as multiplication of Fourier transforms of the signals [15].

$$p_\tau(t) \Leftrightarrow \tau \frac{\sin(\pi\tau f)}{(\pi\tau f)} \tag{2.3}$$

$$\sum_{n=-\infty}^{\infty} \delta(t - nT_r) \Leftrightarrow f_r \sum_{m=-\infty}^{\infty} \delta(f - mf_r) \tag{2.4}$$

$$\begin{aligned} P(f) &= \frac{\tau}{T_r} \frac{\sin(\pi\tau f)}{\pi\tau f} \sum_{m=-\infty}^{\infty} \delta(f - mf_r) \\ &= \frac{\tau}{T_r} \sum_{m=-\infty}^{\infty} \frac{\sin(\pi\tau m f_r)}{\pi\tau m f_r} \delta(f - mf_r) \end{aligned} \tag{2.5}$$

Equation (2.3) shows the spectrum of the pulsed waveform includes discrete spectral lines spaced at the PRF (f_r), and they are weighted with a *sinc* function, where $sinc(x) = sin(\pi x)/(\pi x)$. Equation (2.5) reveals that the *sinc* weighting is determined by the pulsewidth in the spectrum. Thus, the pulsewidth of a PD radar signal only specifies the overall shaping of the spectrum, and it does not affect the location of the spectral lines [15].

In PD radar signal the pulsed waveform given in equation (2.2) is modulated with the continuous complex sinusoid signal to generate transmitted PD radar signal [15]. Thus, an infinite time PD radar signal can be written as equation (2.6)

$$x(t) = p(t)e^{j2\pi f_t t} = \left(p_\tau(t) * \sum_{n=-\infty}^{\infty} \delta(t - nT_r) \right) e^{j2\pi f_t t} \tag{2.6}$$

and its spectrum can be written as equation (2.7) using the Fourier transform pair [15] given in the equation (2.8)

$$X(f) = P(f) * \delta(f - f_t) \tag{2.7}$$

$$= \frac{\tau}{T_r} \sum_{m=-\infty}^{\infty} \frac{\sin(\pi\tau m f_r)}{\pi\tau m f_r} \delta(f - m f_r - f_t)$$

$$e^{j2\pi f_t t} \Leftrightarrow \delta(f - f_t) \tag{2.8}$$

where f_t is the radar transmit frequency. Thus, the spectrum of the infinite time pulse Doppler radar signal is just the spectrum of the pulsed waveform shifted in frequency amount of f_t.

PD radars uses finite time structure due to a limited time-on-target and signal processing limits, so a group of pulses that are to be combined coherently for a limited time is called coherent processing interval (CPI) [14],[15].

An infinite length coherent pulse train has a similar envelope to a single pulse in its spectrum with spectral lines at intervals which are equal to the PRI. However, spectrum of the finite length coherent pulse train consists of finite width spectral lines. There is an inverse proportionality between the length of the coherent pulse train and corresponding spectral lines width [21] (Figure 2.1).

In order to switch from the infinite time assumption to finite time, infinite time PD radar signal, $x(t)$, can be multiplied by a single pulse with a pulsewidth equal to the CPI. Hence, the time limited PD radar signal can be written as,

$$s(t) = p_{\tau_w}(t) x(t) \tag{2.9}$$

$$\begin{aligned} S(f) &= \tau_w \frac{\sin(\pi\tau_w f)}{\pi\tau_w f} * X(f) \\ &= \frac{\tau\tau_w}{T_r} \sum_{m=-\infty}^{\infty} \frac{\sin(\pi\tau m f_r)}{\pi\tau m f_r} \frac{\sin(\pi\tau_w(f - m f_r - f_t))}{\pi\tau_w(f - m f_r - f_t)} \end{aligned} \tag{2.10}$$

Equation (2.10) introduces that the finite time structure changes the each dirac delta function is substituted by a *sinc* function. In the time limited PD radar signal the

length of the CPI (τ_w) determines the width of the individual *sinc* function; with a longer CPI producing a narrower *sinc* function, and shorter CPI causes a wider *sinc* function in the spectrum. In typical PD radar, the CPI can be used as tens to hundreds of pulse repetition intervals (PRI) [15]. Figure 2.2 shows the PD radar signal spectrums for different CPI values, and it is evident that the spectral lines or individual sinc functions get wider when the processed pulse number or CPI (τ_w) value decreases.

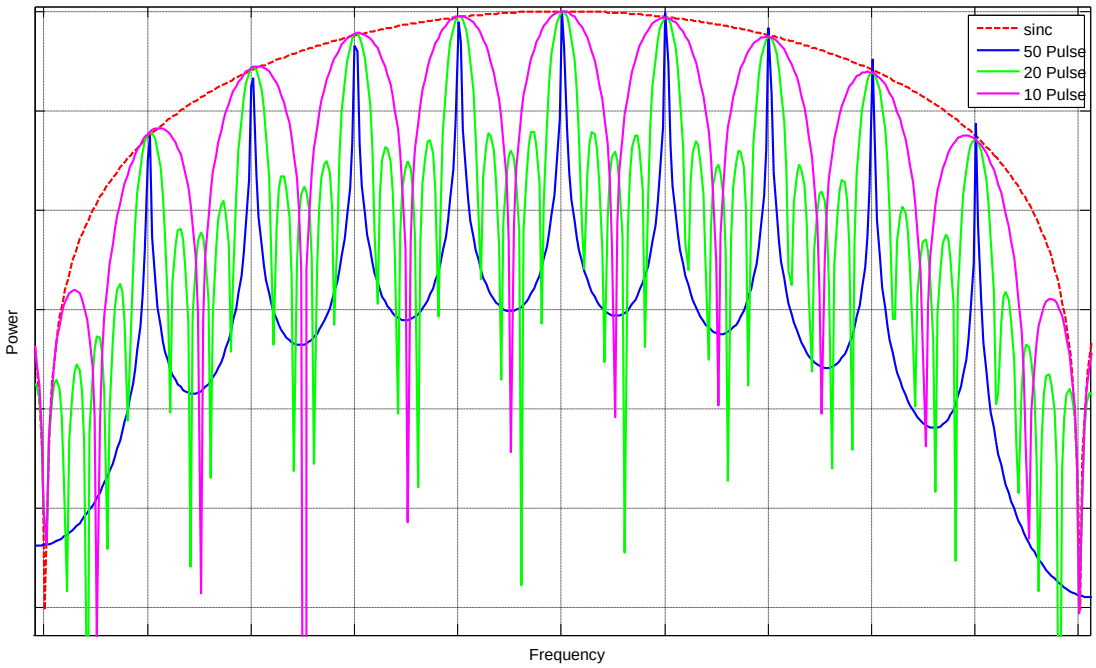

Figure 2.2 CPI effect on PD radar signal

As a brief explanation to generation of PD radar, at the beginning, the pure PD radar signal is a continuous complex sine wave including a dirac delta function located at the radar transmit frequency in the spectrum. After that, this continuous complex sine wave is modulated by a pulsed waveform which provides a frequency spectrum consisting of weighted discrete spectral lines at integer multiples of the PRF around the transmit frequency. This pulsed waveform modulation generates weighting as a *sinc* function whose bandwidth is directly related with pulsewidth. As the final step, the pulse modulated sine wave is limited in time by multiplication with a single pulse which has a pulsewidth equal the CPI. This final step forms the frequency spectrum of discrete spectral lines into *sinc* functions, whose widths are determined by the length of the CPI as the pulse width of the single pulse.

CHAPTER 3

DIGITAL RADIO FREQUENCY MEMORY

Military radars have been widely used as pulse compression, pulse Doppler etc. which are based on coherent radar signal. It was designed to improve radar performance in a clear and natural interference environment, and coherent type radars are proven to be a powerful EP against the older repeater jammer, such as frequency memory loop (FML), based on traditional deception techniques. Because of this reason EW designers developed a system, which stores and repeats a coherent replica of incoming radar signal, that is called digital radio frequency memory (DRFM) [3].

DRFM is a system that is used for storing and recreating radar signals. It improves many of insufficiencies inherent in microwave or frequency memory loops. DRFM provides a memory mechanization which is independent of storage time, and hence removes any deformation of signal fidelity with time delay. DRFM, according to the hardware limits, can store multiple simultaneous signals, and it can replicate as well pulse-compression and phase-coded radar signals [1].

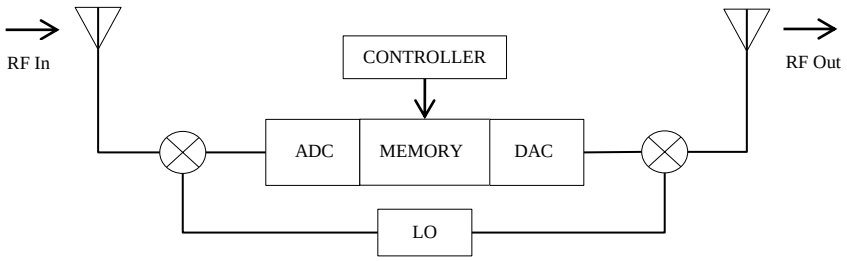

Figure 3.1 DRFM Schematic

A DRFM system basically consists of the following components: a local oscillator (LO), analog-to-digital converter (ADC), high-speed digital memory, digital-to-analog converter (DAC) and a controller unit. Figure 3.1 shows a block diagram of a typical DRFM system [15]. The fundamental task of the DRFM is receiving RF

signal and converting its frequency low enough to be able to sample with a high-speed ADC. The sampled signal is stored in a high-speed memory and can be retrieved and converted back to the original signal using a DAC, and it is up-converted to the received frequency to transmit target radar system.

DRFM device is used in many operational platforms such as aircrafts, frigates etc. to apply EA techniques. The best known EA devices such as EL/L-8222 EW self-protection pod, AN/ALQ-187 EA suite, EWS-39 and AN/ALQ-211 EA systems are fitted to air platforms has DRFM device. Also, SCORPION 2 radar electronic countermeasures system and NETTUNO 4100 EA system which operate on sea platforms are equipped with DRFM. Moreover, today modern off-board EA devices like expandable decoys such as BriteCloud are also equipped with DRFM to apply jamming and deception techniques. Thus, DRFM device is playing an important operational role in today's EW environment. These devices intend target's tracking radars, so they operate generally in C, X and Ku bands. Table 3.1 shows the some capabilities of SCORPION 2 system.

Table 3.1 Capabilities of SCORPION 2 [22]

Frequency Band	7.5 to 18 GHz
Effective Radiated Power (ERP)	100 kW
Technique Generator	DRFM based
Simultaneous Threats	2
Noise Techniques	Pulsed Noise, Cover Noise
Deception Techniques	False Target, RGPO, RGPI

In particular, DRFMs are widely used in EA techniques to generate false radar echoes, which are range false target (RFT), velocity gate pull-off/pull-in (VGPO/I) and range gate-pull off/pull-in (RGPO/I) techniques. RFT and RGPO/I techniques are used to deceive the target radar system in range, VGPO/I technique is used to deceive it in velocity domain. Pull-off (VGPO and RGPO) and pull-in (VGPI and RGPI) techniques are very similar from the implementation point of view. Pull-off techniques are used to send away target's tracking gate from real echo signal while pull-in techniques are used to walk the tracking gate closer than the real echo signal.

RFT technique is effective against search radars and the acquisition phase of tracking radars. It can be used for both self-protection and stand-off jamming by synchronizing with the radar PRF to create a series of false targets in range on the search radar PPI scope [3]. VGPO technique uses CW or pulsed signals to deceive tracking radar considering Doppler effect by changing frequency of received radar signal in time. For effective VGPO implementation, at the beginning, radiated deceptive signals should be at the same frequency with tracking radar to capture the target radar automatic gain controller (AGC). Later, the frequency of the deception signal is changed to pull-off the velocity gate [3].

In the following sections the other EA technique, RGPO, that is used to deceive target tracking radar in range, and its sub-branches (linear and parabolic RGPO techniques) are described, and their mathematical basis are presented.

3.1. Range Gate Pull-Off (RGPO) Technique

Range gate pull-off (RGPO) is a fundamental deceptive EA technique that is used to range jamming to range trackers of tracking radars of hostile forces [3]. It is also known as range gate walk-off or range gate stealing.

Using the RGPO technique, the deception jammer initially repeats the received radar pulse with minimum time delay. This allows the AGC circuitry to adjust to the stronger jammer signal, which has the effect of capturing the radar AGC while reducing the radar's sensitivity with respect to the actual signal. Then, the deception jammer begins to introduce increasing amounts of time delay in the repeated signal. The radar range gate circuitry begins to track the jammer signal which is stronger than the target echo and finally deceptive signal gradually walks-off from the true target range [3]. Figure 3.2 illustrates the steps of the RGPO technique described above.

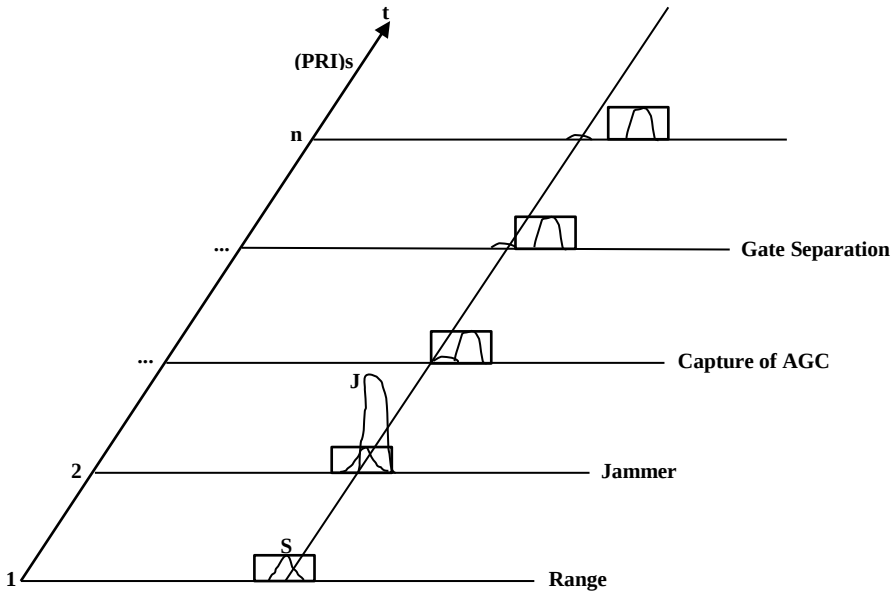

Figure 3.2 Range Gate Pull-Off Technique [3]

In brief, RGPO technique is applied to benefit from weakness of range gate circuits of the tracking radars. In this technique pulses come from the victim's radar are copied and they are retransmitted to the victim's radar with a specific time delay by increasing the amplitude of the copied radar signal. Then, radar assumes that the coming radar echo its own signal echo and it places its range gate on this deceptive signal, so range gate is pulled up to a false target range from the real target range, and radar lose the ability of tracking of the real target [2].

RGPO technique generates a false target which appears at greater range than the real target range since the deceptive RGPO signal is transmitted after the victim radar echo. When applying the RGPO technique without a DRFM, if the PRF of the victim radar is constant, then the time of arrival (TOA) of the next radar pulse can be calculated, and the produced deceptive pulses can be placed at closer or further ranges. On the other hand, PRF of the victim radar is stagger, jitter or dwell/switch type its PRF pattern should be known to deceive the victim radar system. [23]. On the other hand, when the RGPO technique is applied by a DRFM system, then false target is generated without any calculation since the DRFM system copies the victim radar signal and hence its PRF pattern. The PRF pattern is a problem just in the case of applying RGPI technique for a DRFM system, because in the RGPI the deceptive pulse must be transmitted before the victim radar signal echo.

The RGPO technique may be applied as linear or parabolic RGPO according to the pull-off function or movement of the false target. These two pull types are described in the following sections.

3.1.1. Linear Range Gate Pull-Off

During linear RGPO technique, the replicated radar signal by DRFM is transmitted back to the victim radar with a time delay which is incremented linearly with respect to the received radar signal.

The discrete nature of the DRFM causes a time delay on the deceptive pulses with discrete steps at discrete time intervals instead of linearly increasing time delay. So, this discrete behavior causes an RGPO spectrum which has a small center frequency shift and producing spectral lines or harmonics. Another source of harmonics is the discrete nature of the ADC for a DRFM, but it is not discussed in this thesis work presented here. The following analysis, DRFM linear RGPO signal derivations, is collected from the Berger's works [14],[15] about the linear RGPO to compare with the DRFM parabolic RGPO signal derivations.

The input signal of the DRFM is

$$x(t) = p(t)e^{j2\pi f_0 t} = \left(p_\tau(t) * \sum_{n=-\infty}^{\infty} \delta(t - nT_r) \right) e^{j2\pi f_0 t} \tag{3.1}$$

which is same as the previous infinite PD radar signal in equation (2.6) with f_t, radar transmit frequency, replaced with f_0 which represents the addition of radar transmit frequency and Doppler shift because of the radar and target movement. RGPO applied output signal of the DRFM can be represented as the input signal which has a delay function with respect to time given in equation (3.1). So, the output signal of DRFM is given by

$$y(t) = x(t - c(t))$$
$$= \left(p_\tau(t) * \sum_{n=-\infty}^{\infty} \delta(t - nT_r - c(t)) \right) e^{j2\pi f_0 (t - c(t))} \tag{3.2}$$

where $c(t)$ is the time delay function of the RGPO technique which determines the time delay between the received radar signal from target and deceptive transmitted (RGPO applied DRFM output) signals. In other words, the time delay function specifies how the deceptive false target moves in range domain relative to the target radar. In the delayed output signal, total time delay represented by $c(t)$ is small in comparison with PRI, T_r, so the dirac delta function, $\delta(t - nT_r - c(t))$, approximates to $\delta(t - nT_r)$. Hence, the DRFM output signal can be written as

$$y(t) \approx \left(p_\tau(t) * \sum_{n=-\infty}^{\infty} \delta(t - nT_r) \right) e^{j2\pi f_0 (t - c(t))} \tag{3.3}$$

The first term of the equation (3.3) is the same as the pulsed waveform given in equation (2.2). This pulse waveform causes replications of the frequency spectrum of the right-hand side term at multiples of the target radar PRF. So, the frequency spectrum of the exponential signal term in the DRFM output signal has deterministic role in the overall output signal frequency spectrum.

The exponential signal term can be discussed as a separate signal, $d(t)$, as follows:

$$d(t) = e^{j2\pi f_0 (t - c(t))} = e^{j2\pi f_0 t} e^{-j2\pi f_0 c(t)}$$
$$= a(t)b(t) \tag{3.4}$$

and it can be split into two parts where

$$a(t) = e^{j2\pi f_0 t} \tag{3.5}$$

$$b(t) = e^{-j2\pi f_0 c(t)} \tag{3.6}$$

The frequency domain representations of $d(t)$, $a(t)$ and $b(t)$ signals are denoted $D(f)$, $A(f)$ and $B(f)$. The $D(f)$ can be represented as convolution of $A(f)$ and $B(f)$ since multiplication of two time domain signal is represented in frequency domain as convolution of Fourier transforms of the signals, and frequency spectrum is $A(f)$ represented as $\delta(f - f_0)$ [15]. Hence, it can be represented as follow using the equation (3.8) which represents the sifting property of the dirac delta function.

$$D(f) = A(f) * B(f) = B(f - f_0) \tag{3.7}$$

$$x(t) * \delta(t \pm \alpha) = x(t \pm \alpha) \tag{3.8}$$

Thus, the spectrum of DRFM output signal given in equation (3.3) can be reduced to $B(f)$ as given in the equation (3.7).

For an ideal DRFM system, the update rate and time delay resolution can be considered to be infinitely small, and hence, the time delay function of RGPO signal would be a continuous function of time.

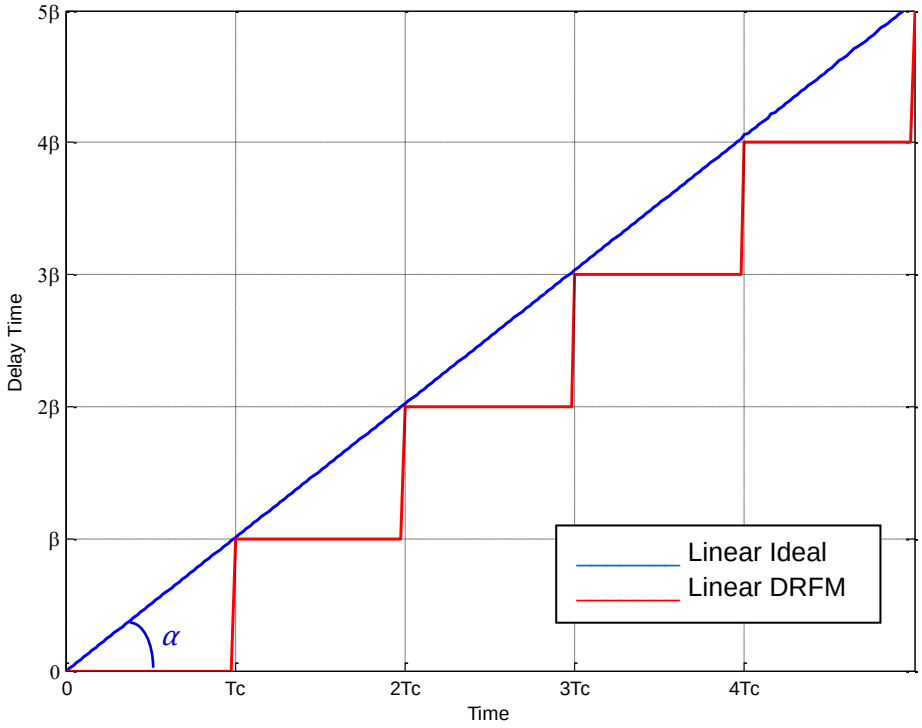

Figure 3.3. Ideal and real linear RGPO pull functions

Therefore, for an ideal DRFM, pull function is $c(t) = \alpha t$ where α is the pull-off rate. For a non-ideal (realistic) DRFM, pull function, $c(t) = r(t)$ where $r(t)$ is a piece-wise continuous function of time that approximates αt with stair-step function, and Figure 3.3 illustrates these ideal and realistic DRFM RGPO time delay functions.

Under ideal conditions, that is $c(t) = \alpha t$, $b(t)$signal can be represented as follows:

$$b(t) = e^{-j2\pi f_0 \alpha t} \tag{3.9}$$

and its spectrum is expressed as the following equation.

$$B(f) = \delta(f + \alpha f_0) \tag{3.10}$$

So that, the frequency spectrum of the ideal RGPO signal from equation (3.7) is

$$D(f) = \delta(f - f_0 + \alpha f_0) \tag{3.11}$$

Equation (3.11) reveals that an ideal linear delay function provides a frequency shift equal to αf_0 as constant.

Using the infinite time assumption, according to the Figure 3.3 the real DRFM linear RGPO time delay function can be represented as a stair-step function as follows.

$$r(t) = \beta \sum_{n=-\infty}^{\infty} np_{T_c}(t - nT_c - T_c/2) \tag{3.12}$$

where n is an integer. The step size (β) and step length (T_c) parameters are determined by the time delay resolution (t_d), update rate (t_s) and pull-off rate (α). The determination of β and T_c is discussed at the end of this section. Using the stepwise representation of the realistic DRFM linear RGPO time delay function given in equation (3.12), real DRFM linear RGPO frequency spectrum can be

derived. Using the time delay function given in equation (3.12) and RGPO signal given in equation (3.6), the real DRFM linear RGPO signal $b(t)$ can be written as

$$b(t) = e^{-j2\pi f_0 \beta \sum_{n=-\infty}^{\infty} n p_{T_c}(t - nT_c - T_c/2)} \tag{3.13}$$

To determine the frequency spectrum of $b(t)$; first, it should be written into a more convenient form. Observe that

$$\beta \sum_{n=-\infty}^{\infty} n p_{T_c}(t - nT_c - T_c/2) = \beta k \tag{3.14}$$

$$\text{for } kT_c < t \leq (k+1)T_c \text{ and } k \in \mathbb{Z}$$

and hence,

$$b(t) = e^{-j2\pi f_0 \beta k} \text{ for } kT_c < t \leq (k+1)T_c \tag{3.15}$$

Next, observe that

$$p_{T_c}(t - nT_c - T_c/2) e^{-j2\pi f_0 \beta k} \tag{3.16}$$

$$= \begin{cases} e^{-j2\pi f_0 \beta k} & kT_c < t \leq (k+1)T_c \\ 0 & otherwise \end{cases} \tag{3.17}$$

Finally, using the equation (3.17), $b(t)$ can be written as

$$\begin{aligned} b(t) &= \sum_{n=-\infty}^{\infty} p_{T_c}(t - nT_c - T_c/2) e^{-j2\pi f_0 \beta n} \\ &= p_{T_c}(t - T_c/2) * \left(\sum_{n=-\infty}^{\infty} e^{-j2\pi f_0 \beta n} \, \delta(t - nT_c) \right) \\ &= p_{T_c}(t - T_c/2) * \left(\sum_{n=-\infty}^{\infty} e^{-j2\pi (f_0 \beta / T_c) n T_c} \, \delta(t - nT_c) \right) \end{aligned} \tag{3.18}$$

$$= p_{T_c}(t - T_c/2) * \left(e^{-j2\pi(f_0\beta/T_c)t} \sum_{n=-\infty}^{\infty} \delta(t - nT_c) \right)$$

$$= w(t) * (v(t)z(t))$$

where

$$w(t) = p_{T_c}(t - T_c/2) \tag{3.19}$$

$$v(t) = e^{-j2\pi(f_0\beta/T_c)t} \tag{3.20}$$

$$z(t) = \sum_{n=-\infty}^{\infty} \delta(t - nT_c) \tag{3.21}$$

From the equation (3.18), the frequency spectrum of $b(t)$ can be written easily as

$$B(f) = W(f)(V(f) * Z(f)) \tag{3.22}$$

The Fourier transforms of $w(t)$, $v(t)$and $z(t)$, are represented as $W(f)$, $V(f)$ and $Z(f)$, and they are given in [15] as below.

$$W(f) = e^{-j\pi f T_c} T_c \frac{\sin(\pi f T_c)}{\pi f T_c} \tag{3.23}$$

$$V(f) = \delta(f + \beta f_0/T_c) = \delta(f + \beta f_0 f_c) \tag{3.24}$$

$$Z(f) = f_c \sum_{n=-\infty}^{\infty} \delta(f - nf_c) \tag{3.25}$$

where f_c represents $1/T_c$. Finally, replacing the equations (3.23)-(3.25) into the equation (3.22) gives

$$B(f) = e^{-j\pi f T_c} T_c \frac{\sin(\pi f T_c)}{\pi f T_c} \left(\delta(f + \beta f_0 f_c) * f_c \sum_{n=-\infty}^{\infty} \delta(f - n f_c) \right)$$

$$= e^{-j\pi f T_c} \frac{\sin(\pi f T_c)}{\pi f T_c} \left(\sum_{n=-\infty}^{\infty} \delta(f + \beta f_0 f_c - n f_c) \right) \tag{3.26}$$

and

$$|B(f)|^2 = \frac{\sin^2(\pi f T_c)}{(\pi f T_c)^2} \left(\sum_{n=-\infty}^{\infty} \delta(f + \beta f_0 f_c - n f_c) \right) \tag{3.27}$$

According to the equation (3.26) and (3.27) DRFM linear RGPO spectrum has spectral lines spaced at f_c and centered at $\beta f_0 f_c$ Hz, and these spectral lines are centered at 0 Hz by weighting a *sinc* function. *Sinc* function in equation (3.26) has nulls at $f = n f_c$ and all spectral lines located at integer multiples of f_c when βf_0 is an integer. In this condition all spectral lines are suppressed except that the spectral line at $f = 0$ Hz, and so $\beta f_0 f_c$ term effects the shift location of the spectral lines away from multiples of f_c. Also, the *sinc* function in equation (3.26) provides a the spectral line which has the largest magnitude always occurs on the interval $-0.5 f_c \leq f \leq 0.5 f_c$. To decide the location of the largest magnitude spectral line, n value should be determined from the inequality such that $-0.5 f_c \leq (-\beta f_0 f_c + n f_c) \leq 0.5 f_c$, and using the following inequalities,

$$-f_c \leq -\beta f_0 f_c + \lfloor \beta f_0 \rfloor f_c \leq 0 \text{ and}$$

$$0 \leq -\beta f_0 f_c + (\lfloor \beta f_0 \rfloor + 1) f_c \leq f_c \tag{3.28}$$

n value is either equal to $\lfloor \beta f_0 \rfloor$ or $\lfloor \beta f_0 \rfloor + 1$, where $\lfloor . \rfloor$ symbol represents the next largest integer operations. n is equal to $\lfloor \beta f_0 \rfloor + 1$, when $-\beta f_0 + \lfloor \beta f_0 \rfloor < 0.5$, and $-f_c < (-\beta f_0 f_c + \lfloor \beta f_0 \rfloor f_c) < 0.5 f_c$. On the other hand, n is equal to $\lfloor \beta f_0 \rfloor$, when $-\beta f_0 + \lfloor \beta f_0 \rfloor > -0.5$, Combining these results,

$$f_p = \begin{cases} (-\beta f_0 + \lfloor \beta f_0 \rfloor) f_c & -\beta f_0 + \lfloor \beta f_0 \rfloor > 0.5 \\ (-\beta f_0 + \lfloor \beta f_0 \rfloor + 1) f_c & otherwise \end{cases} \tag{3.29}$$

where f_p denotes the location of the largest magnitude spectral line and it is refers to the center frequency shift. When βf_0 is an integer, then $f_p = 0$, and another special case occurs when $\beta f_0 = -0.5$. In this case, spectral lines are located at $\pm f_c/2$ with equal magnitude. Finally, f_p can be written for these four conditions as,

$$f_p = \begin{cases} 0 & -\beta f_0 + \lfloor \beta f_0 \rfloor = 0 \\ \pm f_c/2 & -\beta f_0 + \lfloor \beta f_0 \rfloor = 0.5 \\ (-\beta f_0 + \lfloor \beta f_0 \rfloor) f_c & -\beta f_0 + \lfloor \beta f_0 \rfloor > 0.5 \\ (-\beta f_0 + \lfloor \beta f_0 \rfloor + 1) f_c & otherwise \end{cases} \tag{3.30}$$

According to the above analysis the largest magnitude spectral line can be at four different frequencies, and each spectral line or harmonic locates in the spectrum according to the equation (3.31).

$$f = f_p + n f_c, \; n \in \mathbb{Z} \tag{3.31}$$

Equation (3.30) reveals that spacing between the spectral lines is determined by the step length, and the magnitude of the spectral lines is determined by T_c through the *sinc* function. Also, the input radar frequency (f_0), step size (β), and step length (T_c) parameter combination determine the center frequency shift in the spectrum.

To observe the effect of the finite time observation on the DRFM linear RGPO spectrum, the signal $d(t)$ or $a(t)b(t)$ product can be multiplied by $p_{\tau_w}(t)$ which is a single pulse with a pulsewidth equal to the observation time τ_w as represented in equation (3.32). Thus, spectrum of the finite time DRFM linear RGPO signal spectrum is convolution of the $D(f)$, or $B(f - f_0)$ which is given in equation (3.7), and spectrum of the single pulse, or *sinc* function as in the equation (3.33).

$$u(t) = p_{\tau_w}(t) d(t) = p_{\tau_w}(t) a(t) b(t) \tag{3.32}$$

$$U(f) = \tau_w \frac{\sin(\pi \tau_w f)}{\pi \tau_w f} * B(f - f_0) \tag{3.33}$$

The spectrum of $B(f-f_0)$ given in equation (3.26) includes a series of dirac delta function which has frequency spacing as f_c, and center frequency of them is shifted amount of f_0. Thus, by the sifting property of the dirac delta functions, the convolution in equation (3.33) provides a spectrum which has a series of *sinc* functions, and width of the *sinc* functions is determined by the observation time. So, if the observation time τ_w is long compared with the step length (T_c), then the individual *sinc* functions will not interact so much each other in the spectrum, but spectral harmonics will interact each other if the observation time is short. So, this interaction, which is proportional to the observation time, will limit the visibility of the spectral harmonics.

As stated previously in this section, the pulsed nature of the DRFM input signal given in equation (3.1) creates replicas of $U(f)$ in the frequency spectrum at each multiple PRF (f_r) frequency. Hence, linear RGPO output signal spectrum of DRFM, $Y(f)$, as follow

$$Y(f) = \sum_{n=-\infty}^{\infty} U(f - nf_r) \tag{3.34}$$

The spectral lines of $B(f-f_0)$ are weighted by a *sinc* function that is related with the T_c or $1/f_c$, so the bandwidth of $B(f-f_0)$ is depended on step length. Thus, if PRF of the radar is sufficiently greater than f_c, then the replicas of $U(f)$ will not affect each other greatly.

Time delay resolution (t_d) and update period (t_s) are factory based parameters; they are decided by DRFM designer in hardware design according to the radar features and real target dynamics. Time delay resolution parameter should be selected such that at each update, the false target signal does not move outside the radar range gate tracker. In other words, the time delay resolution of the range tracking gate of all interested victim radars to deceive must be considered in selecting the time delay resolution parameter.

After the selection of the time delay resolution, the selection of the update period determines an upper bound on velocity of the false target. So, when selecting t_s parameter, the velocity interval of the jamming platform and desired range of false target must be consider in DRFM design.

As an example suppose that $t_d = 5$ ns and $t_s = 1.5$ ms, then at each update the false target moves 1.5 m from the equation ct_d and the maximum velocity of the false target is 1000 m/s from the equation ct_d/t_s, where c represents the speed of light. Moreover, selection of the parameters t_d and t_s also sets the maximum pull-off rate α_{max}, which is represented as $\alpha_{max} = t_d/t_s$, and thus, $\alpha \leq \alpha_{max}$. Also, in the analysis, step size parameter is selected equal to t_d ($\beta = t_d$) to assure that the deceptive target does not move outside the range tracking gate of the radar, and T_c is set to a multiple of t_s such that $\beta/T_c \leq \alpha$. Hence the step length (T_c) parameter can be set as equation (3.35).

$$T_c = \lceil t_d/(t_s\alpha) \rceil t_s \tag{3.35}$$

CHAPTER 4

PARABOLIC RANGE GATE PULL-OFF

The parabolic RGPO is another pull function applied by DRFM as RGPO technique. During parabolic RGPO operations, repeated radar signal is radiated back to the victim radar with a time delay which is increasing in a quadratic manner with respect to the radar signal time. In the case of linear RGPO operation, repeated signal comes to the victim radar with a linear time delay calculated for the deceptive target linear range-rate consideration. In parabolic RGPO, quadratic increasing time delay results time-varying range-rate on the victim radar, and time-varying range-rate can form accelerating or maneuvering target in the scope of the victim radar.

To observe the parabolic RGPO spectrum the signal of $b(t)$ can be analyzed as different from the linear RGPO signal, because DRFM input, given in the equation (3.1), and output, given in the equations (3.2) and (3.3), signals are the same as the linear RGPO section except $c(t)$ signals. Hence, the DRFM parabolic RGPO derivation can be started to analyze from the ideal DRFM time delay function, $c(t)$, signal as below. Under ideal conditions parabolic RGPO time delay function can be applied as the equation (4.1).

$$c(t) = \varphi t^2 + \alpha t \tag{4.1}$$

where φ is the pull acceleration and α is the pull-off rate.

For this time delay function DRFM parabolic RGPO signal, $b(t)$, can be represented as follow

$$b(t) = e^{-j2\pi f_0(\varphi t^2+\alpha t)} = e^{-j2\pi f_0 \varphi t^2} e^{-j2\pi f_0 \alpha t} \tag{4.2}$$

$b(t)$ signal can be split into two parts

$$b(t) = g(t)h(t) \tag{4.3}$$

where

$$g(t) = e^{-j2\pi f_0 \varphi t^2} \tag{4.4}$$

$$h(t) = e^{-j2\pi f_0 \alpha t} \tag{4.5}$$

$g(t)$ signal is a quadratic complex signal and its frequency spectrum representation can be determined by means of stationary phase principle.

The stationary phase principle (SPP) is used for approximate evaluation of integrals with highly oscillatory integrands; so it can be employed in Fourier transformation of some functions [24]. This method is useful when the signal phase function is continuous and nonlinear [24].

Let $s(t) = A(t)e^{j\theta(t)}$which is given as a signal in amplitude and phase form. $A(t)$is amplitude function and $\theta(t)$ is phase function of $s(t)$. The Fourier transform of this signal,

$$S(f) = \int_{-\infty}^{+\infty} s(t)e^{-j2\,\pi\, ft}dt \tag{4.6}$$

$$S(f) = \int_{-\infty}^{+\infty} A(t)e^{j\theta(t)}e^{-j2\pi ft}dt$$

$$= \int_{-\infty}^{+\infty} A(t)e^{j[\theta(t)-2\,\pi\, ft]}dt \tag{4.7}$$

$$S(f) \equiv \int_{-\infty}^{+\infty} A(t)e^{j\phi(t,f)}dt \tag{4.8}$$

The exact Fourier transform is known for signals having relatively simple phase functions $\theta(t)$. On the other hand, in the SPP a stationary point of the integrand must be defined as a value of $t = t_0$, which is the first time derivative of the integral phase

$\phi'(t_0, f)$, to represent the frequency representation of the signal. Then, for a signal which has highly oscillatory integrands, its frequency domain representation written as follow using the SPP approach according to the [24].

$$S(f) \approx \sqrt{\frac{-\pi}{2\phi''(t_0, f)}} e^{-j\frac{\pi}{4}} s(t_0) e^{j\phi(t_0, f)} \tag{4.9}$$

where $\phi''(t_0, f)$ is second time derivative of $\phi(t, f)$ evaluated at $t = t_0$. Equation (34.9) states that the spectrum consists of fixed complex exponential signal $e^{-j\frac{\pi}{4}}$, the signal of $s(t)$ at point t_0 as $s(t_0)$, and complex exponential with total integral phase at point t_0 is $e^{j\phi(t_0, f)}$. Also, magnitude of the spectrum is inversely proportional to the square root of the rate of change of the frequency $\phi''(t_0, f)$ at the stationary point t_0 [24].

Hence, in the derivation $g(t)$ signal can be represented as

$$g(t) = e^{-jkt^2} \text{ ,where } k = 2\pi f_0 \varphi \tag{4.10}$$

and Fourier transform of the $g(t)$ as equation (4.11)

$$\begin{aligned} G(f) &= \int_{-\infty}^{+\infty} g(t) e^{-j2\pi ft} dt \\ &= \int_{-\infty}^{+\infty} e^{j[-kt^2 - 2\pi ft]} df \end{aligned} \tag{4.11}$$

So, the total integral phase of the $G(f)$ is

$$\phi(t, f) = -kt^2 - 2\pi ft \tag{4.12}$$

First and second derivative of the equation (4.12),

$$\phi'^{(t,f)} = -2kt - 2\pi f \tag{4.13}$$

$$\phi''^{(t,f)} = -2k \tag{4.14}$$

and stationary point t_0 is found from equation (4.15) as equation (4.16)

$$\phi'(t_0, f) = 0 \text{ and } -2kt_0 - 2\pi f = 0 \tag{4.15}$$

$$t_0 = -\pi f/k \tag{4.16}$$

Hence, $G(f)$ can be written, as follows, according to the stationary phase principle and the equation (4.9).

$$G(f) = \sqrt{\frac{\pi}{2\pi f_0 \varphi}}\, e^{j\left(\frac{\pi^2 f^2}{2\pi f_0 \varphi} - \frac{\pi}{4}\right)} \tag{4.17}$$

Also, the complex $h(t)$ signal spectrum given in equation (4.5) can be written as equation (4.18).

$$H(f) = \delta(f + \alpha f_0) \tag{4.18}$$

Finally, the spectrum of the $b(t)$ signal can be represented as convolution of the $G(f)$ and $H(f)$ signals; it gives the shifted form of the $G(f)$ spectrum by the amount of the αf_0 as follows

$$\begin{aligned} B(f) &= G(f) * H(f) \\ &= G(f + \alpha f_0) \end{aligned} \tag{4.19}$$

The ideal parabolic RGPO signal spectrum $D(f)$ can be represented as the equation (4.20) by using the $A(f) = \delta(f - f_0)$, and the sifting property of the dirac delta function.

$$D(f) = A(f) * B(f) = A(f) * G(f + \alpha f_0)$$
$$= G(f - f_0 + \alpha f_0) \tag{4.20}$$

After the derivation of the ideal parabolic RGPO signal and its spectrum, real parabolic RGPO signal can be analyzed. Figure 3.4 illustrates typical ideal and real parabolic RGPO pull functions used in DRFM.

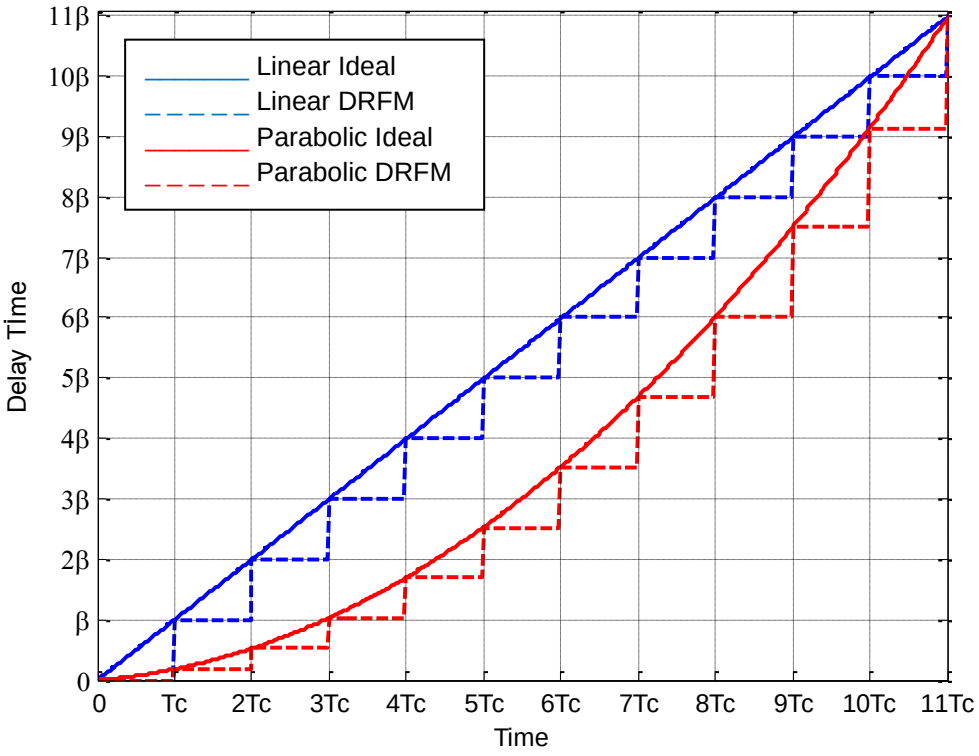

Figure 4.1 Ideal and real parabolic RGPO pull functions

In order to analyze the real DRFM parabolic pull-off function, discrete pull-off function must be represented, and using the infinite time assumption as in the linear RGPO section, the real DRFM parabolic RGPO time delay function can be written as

$$r(t) = \beta \sum_{n=-\infty}^{\infty} (\gamma n^2 + \theta n) p_{T_c}(t - nT_c - T_c/2) \tag{4.21}$$

To understand the frequency spectrum of parabolic RGPO signal, $b(t)$, it can be rewritten into a more convenient form. For this purpose, observe that

$$b(t) = e^{-j2\pi f_0 \beta \sum_{n=-\infty}^{\infty}(\gamma n^2+\theta n) p_{T_c}(t-nT_c-T_c/2)} \tag{4.22}$$

$$b(t) = e^{-j2\pi f_0 \left(\beta\gamma \sum_{n=-\infty}^{\infty} n^2 p_{T_c}(t-nT_c-T_c/2)+\beta\theta \sum_{n=-\infty}^{\infty} n p_{T_c}(t-nT_c-T_c/2)\right)} \tag{4.23}$$

$$\beta\gamma \sum_{n=-\infty}^{\infty} n^2 p_{T_c}(t-nT_c-T_c/2) + \beta\theta \sum_{n=-\infty}^{\infty} n p_{T_c}(t-nT_c-T_c/2) = \beta\gamma k^2 + \beta\theta k \tag{4.24}$$

$$\text{for } kT_c < t \leq (k+1)T_c \text{ and } k \in Z$$

and hence,

$$\begin{aligned} b(t) &= e^{-j2\pi f_0 (\beta\gamma k^2+\beta\theta k)} \\ &= e^{-j2\pi f_0 \beta\gamma k^2} e^{-j2\pi f_0 \beta\theta k} \end{aligned} \qquad \text{for } kT_c < t \leq (k+1)T_c \tag{4.25}$$

Next, observe that

$$p_{T_c}(t-nT_c-T_c/2) e^{-j2\pi f_0 \beta\gamma k^2} e^{-j2\pi f_0 \beta\theta k} \tag{4.26}$$

$$= \begin{cases} e^{-j2\pi f_0 \beta\gamma k^2} e^{-j2\pi f_0 \beta\theta k} & kT_c < t \leq (k+1)T_c \\ 0 & otherwise \end{cases}$$

Finally using equation (4.22), parabolic RGPO signal, $b(t)$, can be written as follows

$$\begin{aligned} b(t) &= \sum_{n=-\infty}^{\infty} p_{T_c}(t-nT_c-T_c/2) e^{-j2\pi f_0 (\beta\gamma n^2+\beta\theta n)} \\ &= p_{T_c}(t-T_c/2) * \left(\sum_{n=-\infty}^{\infty} e^{-j2\pi f_0 \beta\gamma n^2} e^{-j2\pi f_0 \beta\theta n} \delta(t-nT_c) \right) \\ &= p_{T_c}(t-T_c/2) * \left(\sum_{n=-\infty}^{\infty} e^{-j2\pi (f_0 \beta\gamma/{T_c}^2) n^2 {T_c}^2} e^{-j2\pi (f_0 \beta\theta/T_c) n T_c} \delta(t-nT_c) \right) \\ &= p_{T_c}(t-T_c/2) * \left(e^{-j2\pi (f_0 \beta\gamma/{T_c}^2) t^2} e^{-j2\pi (f_0 \beta\theta/T_c) t} \sum_{n=-\infty}^{\infty} \delta(t-nT_c) \right) \\ &= w(t) * (y(t) v(t) z(t)) \end{aligned} \tag{4.27}$$

where

$$w(t) = p_{T_c}(t - T_c/2) \tag{4.28}$$

$$y(t) = e^{-j2\pi(f_0\beta\gamma/{T_c}^2)t^2} \tag{4.29}$$

$$v(t) = e^{-j2\pi(f_0\beta\theta/T_c)t} \tag{4.30}$$

$$z(t) = \sum_{n=-\infty}^{\infty} \delta(t - nT_c) \tag{4.31}$$

From equation (4.27), the frequency spectrum of $b(t)$ can be written as follow

$$B(f) = W(f)(Y(f) * V(f) * Z(f)) \tag{4.32}$$

where $W(f)$, $Y(f)$, $V(f)$ and $Z(f)$ are the Fourier transforms of $w(t)$, $y(t)$, $v(t)$ and $z(t)$, and are given by

$$W(f) = e^{-j\pi f T_c} T_c \frac{\sin(\pi f T_c)}{\pi f T_c} \tag{4.33}$$

$$Y(f) = \sqrt{\frac{\pi {T_c}^2}{2\pi f_0 \beta\gamma}} e^{j\left(\frac{\pi^2 f^2 {T_c}^2}{2\pi f_0\beta\gamma} - \frac{\pi}{4}\right)} \tag{4.34}$$

$$= \sqrt{\frac{1}{2\pi f_0 {f_c}^2 \beta\gamma}} e^{j\left(\frac{\pi^2 f^2}{2\pi f_0 {f_c}^2 \beta\gamma} - \frac{\pi}{4}\right)}$$

$$V(f) = \delta(f + \beta\theta f_0/T_c) = \delta(f + \beta\theta f_0 f_c) \tag{4.35}$$

$$Z(f) = f_c \sum_{n=-\infty}^{\infty} \delta(f - nf_c) \tag{4.36}$$

$Y(f) * V(f) * Z(f)$, is split into two parts as $Y(f)$ and $V(f) * Z(f)$

$$V(f) * Z(f) = \delta\left(f + \beta\theta f_0 f_c\right) * f_c \sum_{n=-\infty}^{\infty} \delta(f - nf_c)$$

$$= f_c \sum_{n=-\infty}^{\infty} \delta(f + \beta\theta f_0 f_c - nf_c) \tag{4.37}$$

and this two parts convolved with each other as follows

$$Y(f) * V(f) * Z(f) = Y(f) * f_c \sum_{n=-\infty}^{\infty} \delta(f + \beta\theta f_0 f_c - nf_c)$$

$$= f_c \sum_{n=-\infty}^{\infty} Y(f + \beta\theta f_0 f_c - nf_c) \tag{4.38}$$

Hence, frequency spectrum of parabolic RGPO signal $b(t)$ is multiplication of $W(f)$ and $Y(f) * V(f) * Z(f)$ as follows

$$\begin{aligned} B(f) &= W(f)(Y(f) * V(f) * Z(f)) \\ &= e^{-j\pi f T_c} T_c \frac{\sin(\pi f T_c)}{\pi f T_c} \left(f_c \sum_{n=-\infty}^{\infty} Y(f + \beta\theta f_0 f_c - nf_c) \right) \\ &= e^{-j\pi f T_c} T_c \frac{\sin(\pi f T_c)}{\pi f T_c} \left(\sum_{n=-\infty}^{\infty} \sqrt{\frac{1}{2 f_0 {f_c}^2 \beta\gamma}}\, e^{j\left(\frac{\pi(f+\beta\theta f_0 f_c - nf_c)^2}{2 f_0 {f_c}^2 \beta\gamma} - \frac{\pi}{4}\right)} \right) \\ &= e^{-j\pi f T_c} \frac{\sin(\pi f T_c)}{\pi f T_c} \left(\sqrt{\frac{1}{2 f_0 {f_c}^2 \beta\gamma}}\, e^{-j\frac{\pi}{4}} \sum_{n=-\infty}^{\infty} e^{j\left(\frac{\pi(f+\beta\theta f_0 f_c - nf_c)^2}{2 f_0 {f_c}^2 \beta\gamma}\right)} \right) \end{aligned} \tag{4.39}$$

According to the equation (4.39) DRFM parabolic RGPO spectrum has series of oscillatory complex exponential parts, while linear RGPO spectrum has spectral lines. This summation of complex exponentials is weighted by a *sinc* function which has a bandwidth of $2f_c$ and it has nulls at multiples of f_c. Also, this signal is multiplied by a constant which is related with the f_0, f_c, step size (β) and discrete pull acceleration (γ) parameters.

Finally, effect of the observation time and pulsed waveform on the DRFM parabolic RGPO signal can be examined. $d(t)$ signal in equation (3.4) can be multiplied by a τ_w, which is the observation time, length pulse $p_{\tau_w}(t)$ as in the linear RGPO section to observe the effect of the finite time observation on the DRFM parabolic RGPO spectrum. Thus, spectrum of the finite time DRFM parabolic RGPO spectrum as

$$U(f) = \tau_w \frac{\sin(\pi\tau_w f)}{\pi\tau_w f} * B(f - f_0) \tag{4.40}$$

The spectrum of $B(f - f_0)$ includes a summation of complex sinusoidal signals by shifted amount of f_0. The *sinc* component coming from the pulsed waveform, or observation time, determines the final spectrum of the parabolic RGPO signal.

$$Y(f) = \sum_{n=-\infty}^{\infty} U(f - nf_r) \tag{4.41}$$

The pulse signal in the DRFM input signal given in the equation (3.1) must be also applied to parabolic RGPO signal. This pulse signal creates replicas of $U(f)$ in the spectrum at each multiple of PRF (f_r) frequency as in the linear RGPO signal derivation. Hence, parabolic RGPO output signal spectrum of DRFM, $Y(f)$ can be written as equation (4.41).

CHAPTER 5

ANALYSIS AND SIMULATION RESULTS

In this chapter, the results of several computer simulations are presented for both linear and parabolic RGPO techniques to verify the validity of the derivations represented in the previous chapter. In the simulations different pull-off cases are simulated to show the effect of the pull function on spectrum for linear and parabolic RGPO techniques. Also, in some scenarios, different DRFM parameters are used to observe the effect of the device parameters for both RGPO techniques.

A typical X-band tracking radar has a pulsewidth of 1 μs and PRF of 1 kHz, and CPI value can be chosen tens to hundreds of PRI or 1/PRF as mentioned before. So, in the simulations the CPI is used as 1024 samples or 102.4 ms. Also, in the simulation of this work 10 kHz sampling rate and 2048 point FFT are used with the Hanning windowing as in the Berger's study [15].

In the simulations, for both linear and parabolic RGPO scenarios, the signal spectrum for 102.4 ms CPI value is compared with two different signal spectrums whose CPI values are 256 samples (25.6 ms) and 128 samples (12.8 ms).

In the following subsections the simulation results are given under linear RGPO scenarios and parabolic RGPO scenarios titles.

5.1. Linear RGPO Scenarios

For the linear RGPO technique different pull-off rate is run and results are presented in this section. Five different scenarios are simulated and analyzed. The first three linear RGPO scenarios are simulated with the same center frequency (operating

frequency), delay resolution and update period parameters, and three different pull-off rates. Fourth scenario is tried for smaller delay resolution and update period with the same pull-off rate and center frequency. Finally, the last scenario has a different center frequency and all other parameters (center frequency, delay resolution, update period) are the same with the first three scenarios. Thus, in this section the spectrums of the linear RGPO signals, which have different RGPO, device or radar parameters, are explained with the following five scenarios. The parameter sets for these scenarios are given in Table 5.1.

Table 5.1 DRFM linear RGPO scenario parameters

	Delay Resolution (t_d) (ns)	**Update Period (t_s) (ms)**	**Pull-Off Rate (α) x10^{-6}**	**Step Length (T_c) (ms)**	**Center Frequency (f_o) (GHz)**
Case 1*	4.44	1.5	1	4.5	9.655
Case 2*	4.44	1.5	0.75	6	9.655
Case 3	4.44	1.5	0.5	9	9.655
Case 4	2.22	0.75	1	2.25	9.655
Case 5	4.44	1.5	1	4.5	9.68468

*Cases from [15].

First three scenarios are determined all together to observe the spectrum changes when DRFM linear RGPO pull-off rate parameter is changed while other parameters are the same. Figure 5.1 shows the ideal and discrete pull-off functions of case 1, 2 and 3.

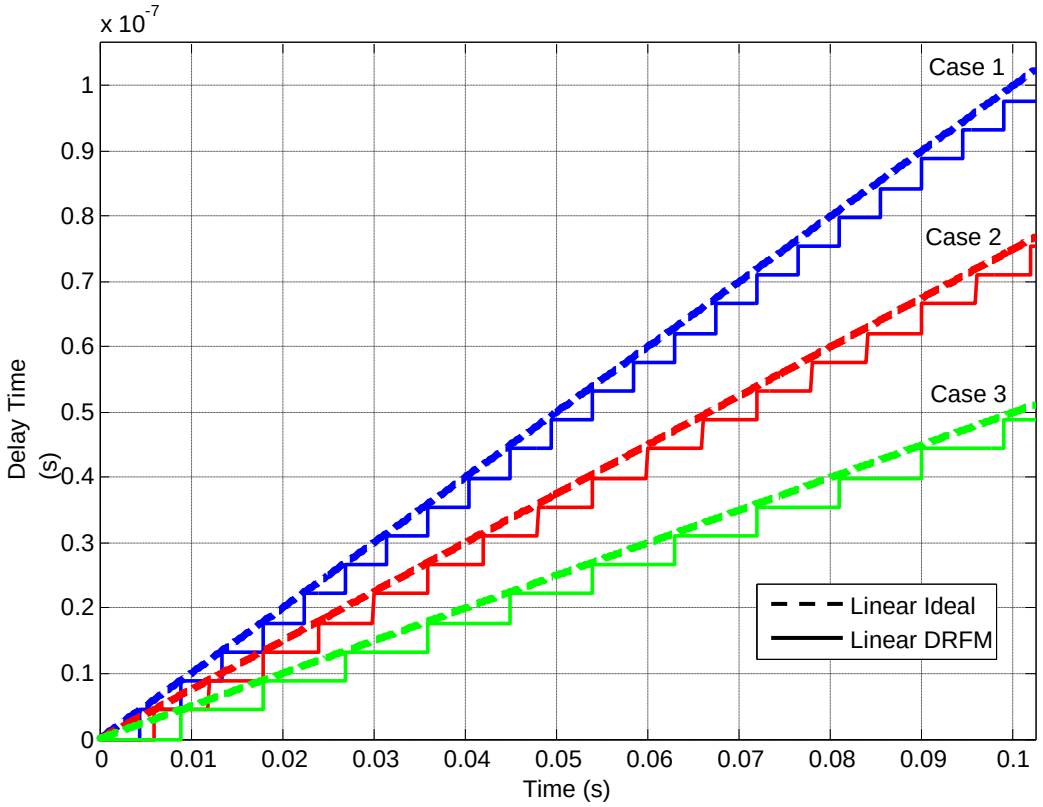

Figure 5.1 Discrete and real linear pull-off functions for cases 1, 2 and 3

In these scenario cases radar center frequency and CPI value are used as 9.655 GHz and 102.4 ms respectively. Also, delay resolution parameter and update period parameter are used as $t_d = 4.44$ ns and $t_s = 1.5$ ms for these three scenarios with three different pull-off rates. According to the equation (3.35), different pull-off rates cause different step lengths for these scenarios. Hence, the frequency between the spectral harmonics changes according to the pull-off rate. In case 1, the DRFM linear RGPO has a maximum delay of 10 μs and walk time of 10 s, which yields a pull-off rate of $\alpha = 1 \times 10^{-6}$. From the equation (3.35) with $t_d = 4.44$ ns, $t_s = 1.5$ ms, and $\alpha = 1 \times 10^{-6}$, the step length parameter is obtained as $T_c = 4.5$ ms. Thus, the predicted spectral line spacing is $f_c = 222.2$ Hz. In case 2, the linear RGPO has a maximum delay of 6 μs and a walk time of 8 s. According to equation (3.35) using t_d, t_s, and α, T_c is obtained 6 ms, so the predicted spectral line spacing is $f_c = 166.7$ Hz for the second scenario. Finally, for case 3, the DRFM linear RGPO has a maximum delay of 5 μs and walk time of 10 s, and step length for this case is used as $T_c = 9$ ms, so the predicted spectral line spacing is $f_c = 111.1$ Hz. The predicted and simulated harmonic offset frequencies are listed in Table 5.2.

Figure 5.2 shows the spectrum of the continuous (or ideal) pull-off function which is represented in Figure 5.1 for case 1, 2 and 3. For the continuous pull-off function the spectrum is represented as a shifted dirac delta function as equation (3.10) for infinite time length signal, but it is a *sinc* function at that frequency for finite time length signal.

In the scenario 1, the center frequency is expected at -9655 Hz as a *sinc* function because of the limited CPI for the continuous pull-off function spectrum with $\alpha = 1 \times 10^{-6}$ and 9.655 GHz radar transmit frequency. Hence, as shown in Figure 5.2 the spectrum center frequency appears at -9652 Hz for this scenario. In case 2, for the continuous pull-off function spectrum, the center frequency is expected at -7241 Hz and it is obtained at -7242 Hz. Finally, for case 3 scenario, the center frequency of continuous pull-off function is expected at -4827 Hz and it appears at -4824 Hz for case 3 (Figure 5.2).

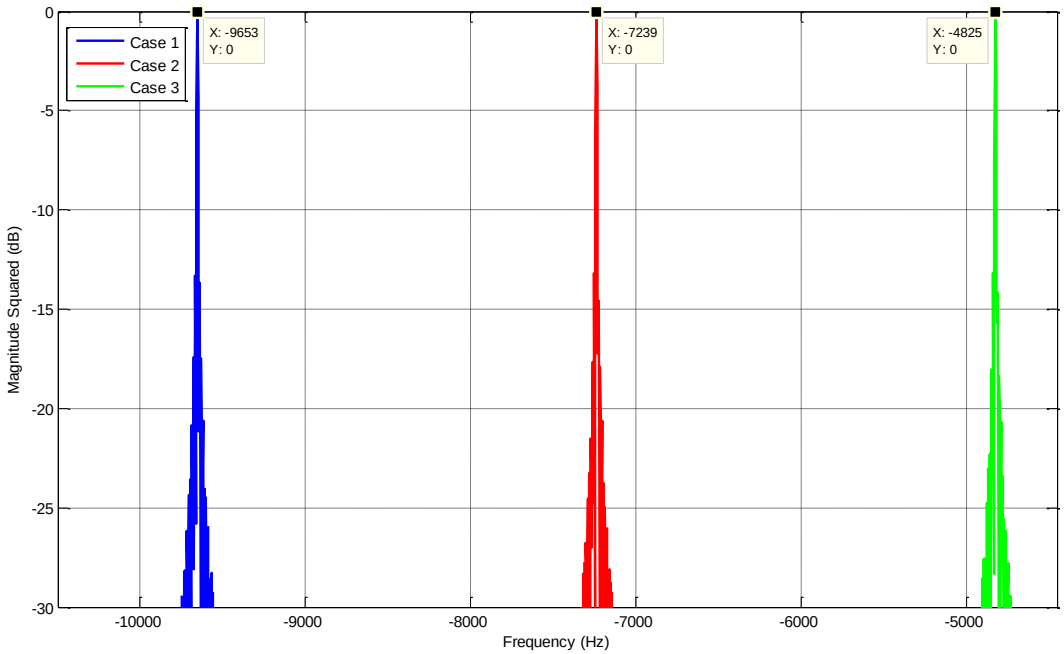

Figure 5.2 Continuous linear pull-off function spectrums for case 1, 2 and 3

Figure 5.3 shows the result of simulated spectrum for case 1, case 2 and case 3 for discrete time pull-off function represented in the Figure 5.1. According to the discrete time linear RGPO derivations in equations (3.26, 3.27), spectrum has spectral lines separated from each other in the amount of f_c or $1/T_c$. Also, it has

central frequency shift, f_p, according to the equation (3.30). Hence, the predicted frequency shift is calculated as $f_p = 29.3$ Hz, and the central frequency shift f_p is obtained as 31.75 Hz in the simulation. First spectral harmonic (right and left) is 224.75 Hz and second spectral harmonic is obtained at 444.55 Hz for the case 1 linear RGPO scenario. For case 2, from simulation results the center frequency shift f_p is obtained as 24.44 Hz, first spectral harmonic is approximately 166.14 Hz and second spectral harmonic is obtained approximately 332.34 Hz however the predicted frequency shift from the equation (3.30) is calculated as $f_p = 21.97$ Hz. Finally, for case 3 linear RGPO scenario, the predicted frequency shift from the equation (3.30) is calculated as $f_p = 14.64$ Hz, and from simulation f_p is acquired as 17.1 Hz, first and second spectral harmonics are obtained approximately as 112.36 Hz and 219.8 Hz. The predicted and simulated center shift and harmonic frequencies are listed in Table 5.2.

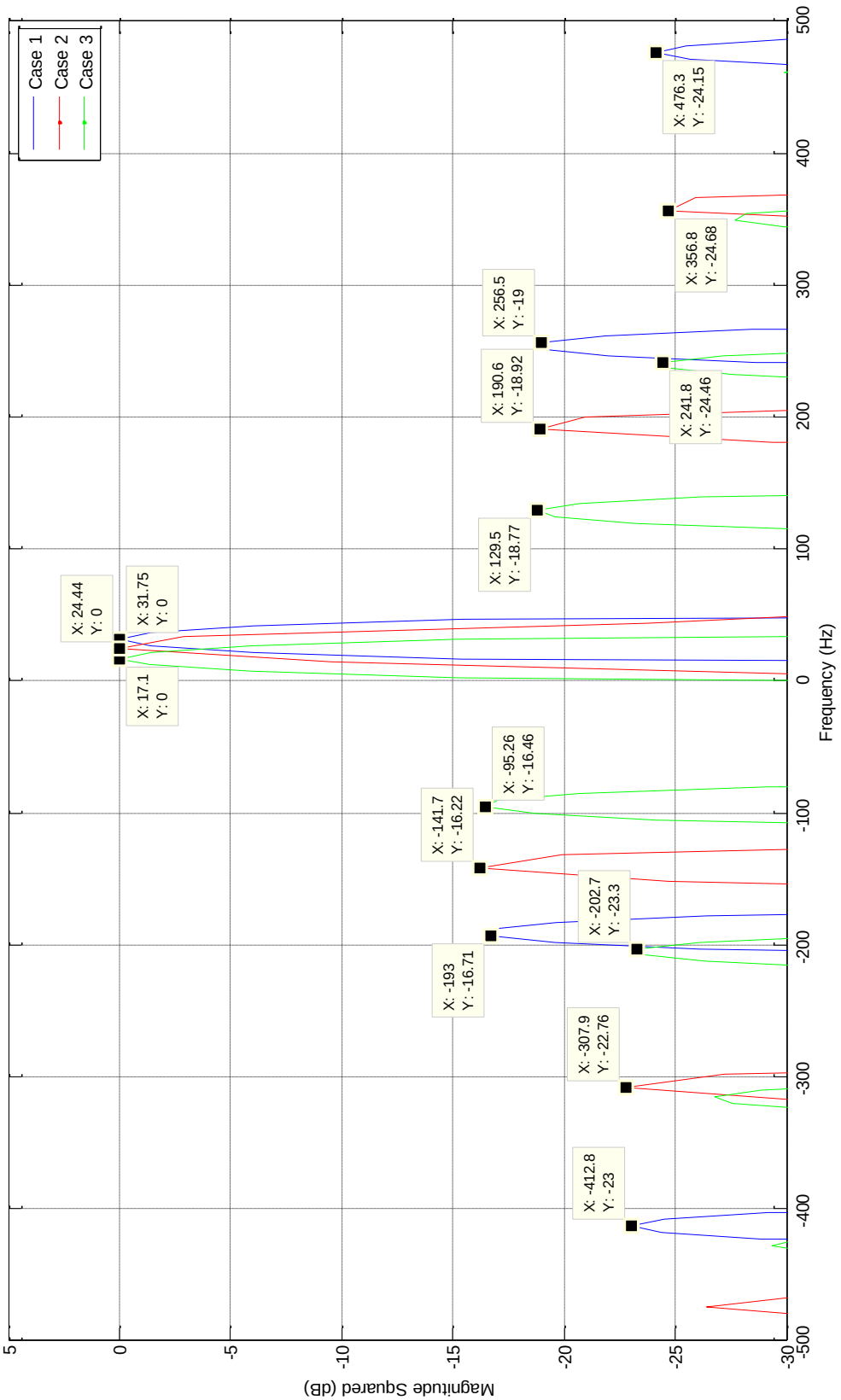

Figure 5.3 Discrete linear pull-off function spectrums for case 1, 2 and 3

Table 5.2 Predicted and simulated results for linear RGPO scenarios

Case 1*	**Predicted Results**		**Simulated Results**	
Center Shift (Hz)	29.3		31.75	
Harmonic	**Offset (Hz)**	**Magnitude (dBc)**	**Offset (Hz)**	**Magnitude (dBc)**
1st Left	222.2	16.36	224.75	16.71
1st Right	222.2	18.68	224.75	19.0
2nd Left	444.4	23.01	444.55	23.0
2nd Right	444.4	24.18	444.55	24.1
Case 2*	**Predicted Results**		**Simulated Results**	
Center Shift (Hz)	21.97		24.44	
Harmonic	**Offset (Hz)**	**Magnitude (dBc)**	**Offset (Hz)**	**Magnitude (dBc)**
1st Left	166.7	16.38	166.14	16.22
1st Right	166.7	18.66	166.16	18.92
2nd Left	333.4	23.05	332.34	22.76
2nd Right	333.4	24.15	332.36	24.68
Case 3	**Predicted Results**		**Simulated Results**	
Center Shift (Hz)	14.64		17.1	
Harmonic	**Offset (Hz)**	**Magnitude (dBc)**	**Offset (Hz)**	**Magnitude (dBc)**
1st Left	111.1	16.37	112.36	16.46
1st Right	111.1	18.68	112.4	18.77
2nd Left	222.2	23.02	219.8	23.3
2nd Right	222.2	24.19	224.7	24.46
Case 4	**Predicted Results**		**Simulated Results**	
Center Shift (Hz)	-193		-191.7	
Harmonic	**Offset (Hz)**	**Magnitude (dBc)**	**Offset (Hz)**	**Magnitude (dBc)**
1st Left	444.4	10.38	444.4	10.37
1st Right	444.4	2.29	444.4	2.302
2nd Left	888.8	14.97	889.3	14.94
2nd Right	888.8	11.14	888.9	11.13

*Cases from [15].

In case 4, the DRFM linear RGPO has a maximum delay of 10 μs and walk time of 10 s, which yields a pull-off rate of $\alpha = 1 \times 10^{-6}$. In this simulation, $t_d = 2.22$ ns and $t_s = 0.75$ ms are used different from scenario 1. So, step length and the predicted spectral line spacing are obtained as $T_c = 2.25$ ms and $f_c = 444.4$ Hz for this scenario. The predicted frequency shift from equation (3.30) is $f_p = -193$ Hz. The predicted and simulated center shift and harmonic offset frequencies are listed in Table 5.2 for case 4.

As mentioned before, case 4 has same scenario parameters with case 1 except delay resolution (t_d) and update period (t_s) parameters. It is simulated with the same transmit frequency and pull-off rate with lower t_d and t_s, so the expected continuous pull-off function spectrum same as case 1 whose center frequency is at the frequency of -9655 Hz.

The result of simulated spectrum for case 4 for discrete time pull-off function represented in Figure 5.4. The central frequency shift f_p is get -191.7 Hz, first spectral harmonic is 444.4 Hz and second spectral harmonic is get 888.9 Hz and 889.3 Hz for case 4 linear RGPO scenario.

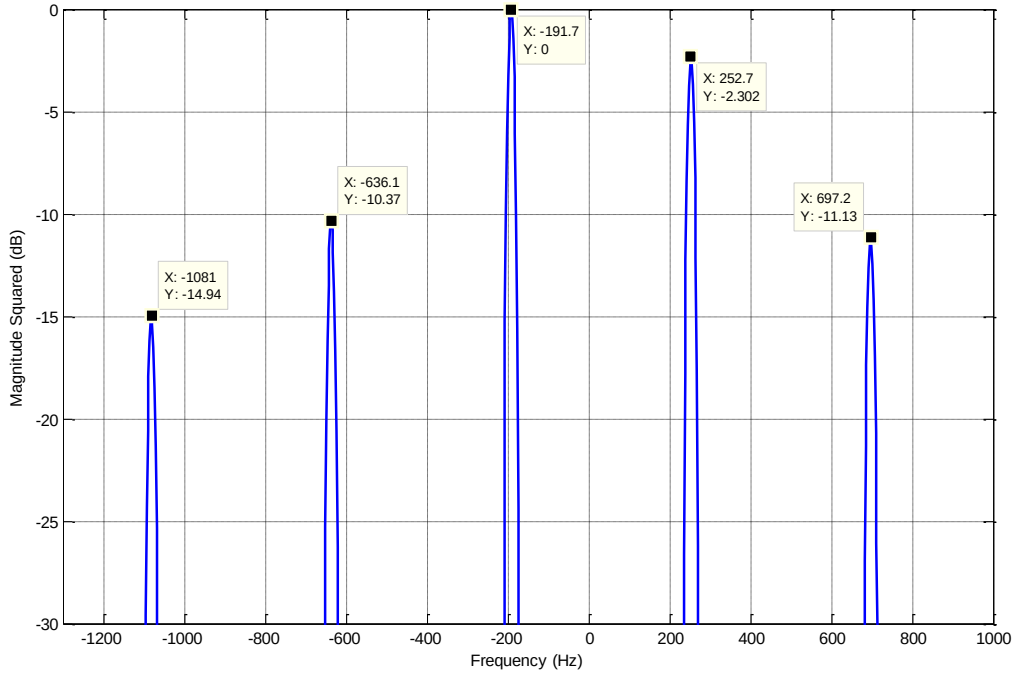

Figure 4.4 Discrete linear pull-off function spectrum for case 4

For the explained DRFM linear RGPO scenarios predicted and simulated center frequency shifts, offsets of the first and second harmonics and their magnitudes all are listed in Table 5.2. According to the predicted and simulated results, approximate frequency error of 2.5 Hz and maximum magnitude error of 0.5 dB are observed. In the simulations, the resource of the error is attributed to the size of FFT. The simulation results for higher FFT point are given in Appendix part, and they show the predicted center frequency shift, harmonic offset and magnitude values are closely matched when simulation FFT value is chosen higher.

Finally, in case 5, the DRFM linear RGPO has a maximum delay of 10 μs and walk time of 10 s, which yields a pull-off rate of $\alpha = 1 \times 10^{-6}$. In this scenario the radar center frequency is 9.68468 GHz and 102.4 ms CPI value is used. The predicted frequency shift $f_p = 0$ Hz, since $-\beta f_0 + \lfloor \beta f_0 \rfloor = 0$ from equation (3.30), and using equation (3.35) delay resolution $t_d = 4.44$ ns, update period $t_s = 1.5$ ms, and pull-off rate $\alpha = 1 \times 10^{-6}$, gives us $T_c = 4.5$ ms and thus, the predicted spectral line spacing is $f_c = 222.2$ Hz. This scenario is tried to show there is no frequency shift in the spectrum when the radar and DRFM parameters is chosen in appropriate way. So, just the radar transmit frequency is changed as different from scenario 1 according to the equation (3.30) zero frequency shift condition. Hence, the continuous and discrete pull-off functions is applied as case 1 in Figure 5.1, and according to the equation (3.10) the continuous pull-off function spectrum is expected at -9684 Hz with $\alpha = 1 \times 10^{-6}$ and changed 9.68468 GHz transmit frequency, f_0; in the simulation run the center frequency appears at -9686 Hz as shown in Figure 5.5.

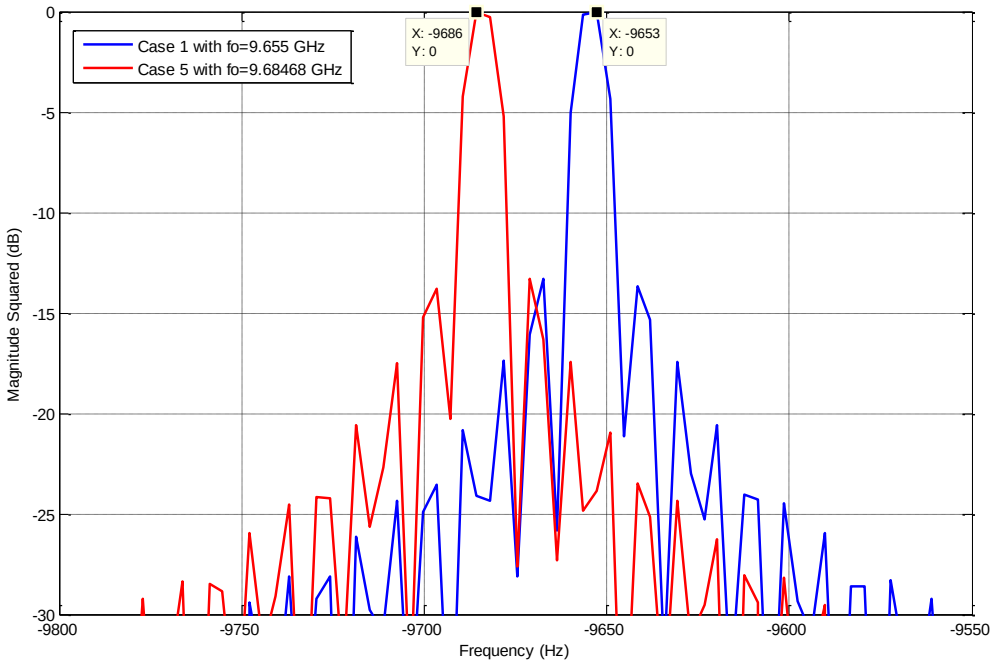

Figure 5.5 Continuous pull-off function spectrums for case 1 and 5

Figure 5.6 shows the spectrum of the zero frequency shift case for discrete time linear RGPO function. The spectrum is expected at 0 Hz, but it is slightly shifted version of the expected spectrum (at 2.443 Hz) because of the low FFT value as in the previous scenarios.

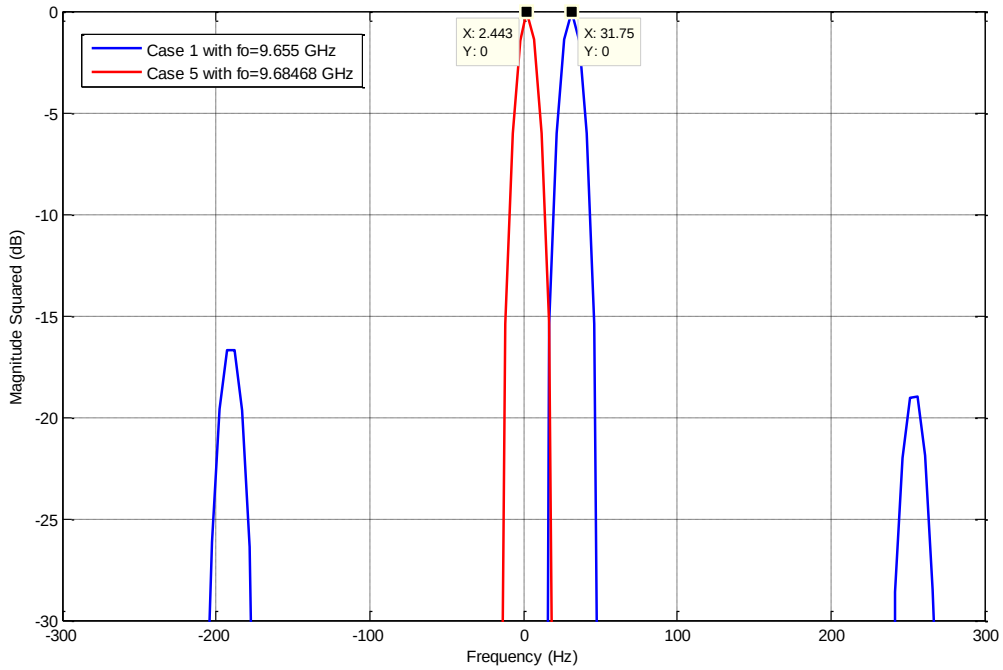

Figure 5.6 Discrete linear pull-off function spectrums for case 1 and 5

As noted in the previous chapter, the length of the CPI, in other words the observation time, determines the width of the spectral lines. In the above cases the used CPI value is 102.4 ms. Here, shorter CPI values are simulated to get wider spectral lines, and to show decreasing the ability to observe the individual spectral lines. The parameters used in this simulation are the same as in scenario 1, except that two shorter CPIs (256 samples or 25.6 ms, and 128 samples or 12.8 ms). As described in PD radar signal, theoretically RGPO applied signal, which has long CPI value, has better spectrum visibility than the spectrum of the signal which has shorter CPI since long CPI signal produces the narrower spectral lines. Figure 5.7 shows the DRFM linear RGPO signal spectrums, which have different CPIs (102.4 ms, 25.6 ms and 12.8 ms), all together to compare effects of CPI value. As shown in this figure, the spectrum of the signal whose CPI is 12.8 ms have widest spectral lines with respect to the others. Therefore, Figure 5.7 shows that the spectral lines are hardly visible for shortest CPI value, but the visibility of the spectral lines improve when the CPI value gets longer.

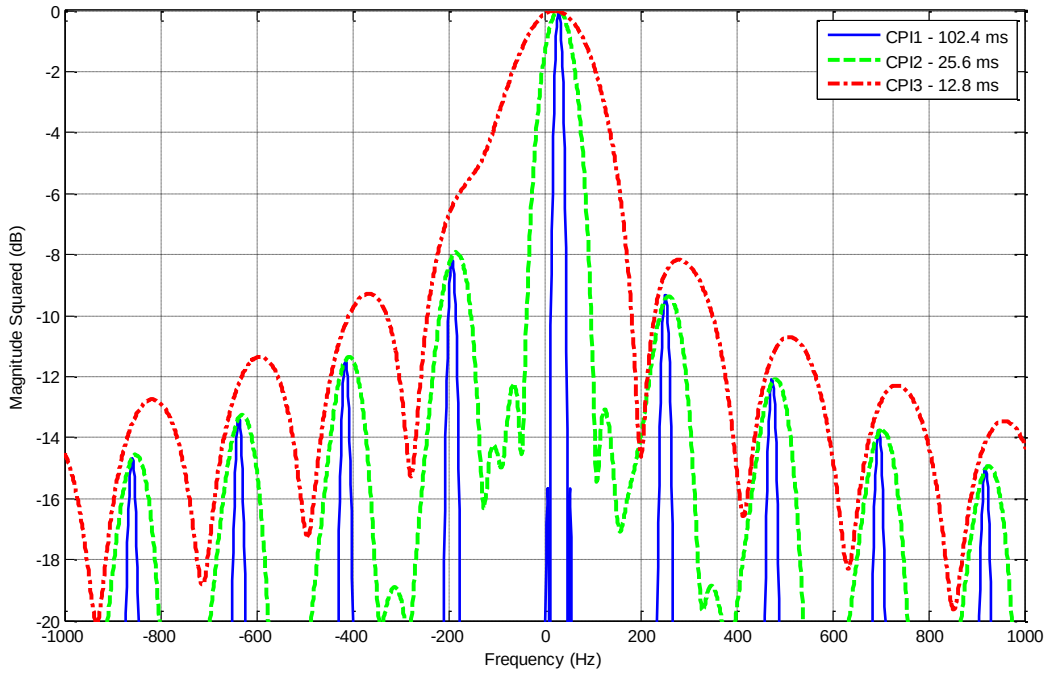

Figure 5.7 Discrete linear pull-off function spectrums for case 1 for all CPI values.

5.2. Parabolic RGPO Scenarios

For the parabolic RGPO technique, variation of pull-off rate and pull acceleration is studied and simulation and results are presented in this section. Five different parabolic RGPO scenarios are studied and analyzed. The first three scenarios are simulated with the fixed parameter set (radar center frequency, CPI, delay resolution and update period parameters) except that the pull-off rate and pull acceleration to observe the spectrum differences when the pull function is varied. Fourth case is run as a control scenario to show the parabolic RGPO spectrum turns into a linear RGPO spectrum when the pull acceleration parameter is zero. Finally, the last scenario shows how the parabolic RGPO spectrum changes when the DRFM delay resolution and update period parameters are selected smaller while the other parameters are fixed. Additionally step length parameter (T_c) determined by the equation (3.35) is used as in the linear RGPO derivation to compare the results of the parabolic and linear RGPO, and it is evaluated that the pull-off techniques are applied with the same DRFM hardware, so in the first four scenarios, step length is used as $T_c = 4.5$ ms. The scenario 5 is simulated with smaller t_d and t_s parameters and hence smaller

T_c, to show the effect of the step length on the parabolic RGPO spectrum as in the linear RGPO section. Parameter sets for these five parabolic RGPO scenarios are listed in Table 5.3.

Table 5.3 DRFM parabolic RGPO scenario parameters

	Delay Resolution (t_d) (ns)	**Update Period (t_s) (ms)**	**Pull-Off Rate (α) x10^{-6}**	**Pull Acceleration (φ) x10^{-6}**	**Step Length (T_c) (ms)**
Case 1	4.44	1.5	0.05	9.277	4.5
Case 2	4.44	1.5	0.5	4.883	4.5
Case 3	4.44	1.5	0.92	0.78125	4.5
Case 4	4.44	1.5	1	0	4.5
Case 5	2.22	0.75	0.05	9.277	2.25

First three scenarios are determined all together to observe the spectrum changes when DRFM parabolic RGPO pull-off rate and pull acceleration parameters are varied, but all other parameters are fixed; in other words, radar center frequency (9.655 GHz), CPI (102.4 ms), delay resolution (4.44 ns) and update period (1.5 ms) parameters are fixed for these scenarios. Figure 5.8 shows the ideal and discrete pull functions of the case 1, 2 and 3. Also, in this figure parabolic pull functions are represented with the linear continuous (ideal) pull function has $\alpha = 1 \times 10^{-6}$ and same CPI (102.4 ms) to compare behaviors of the parabolic pull functions with respect to linear pull function.

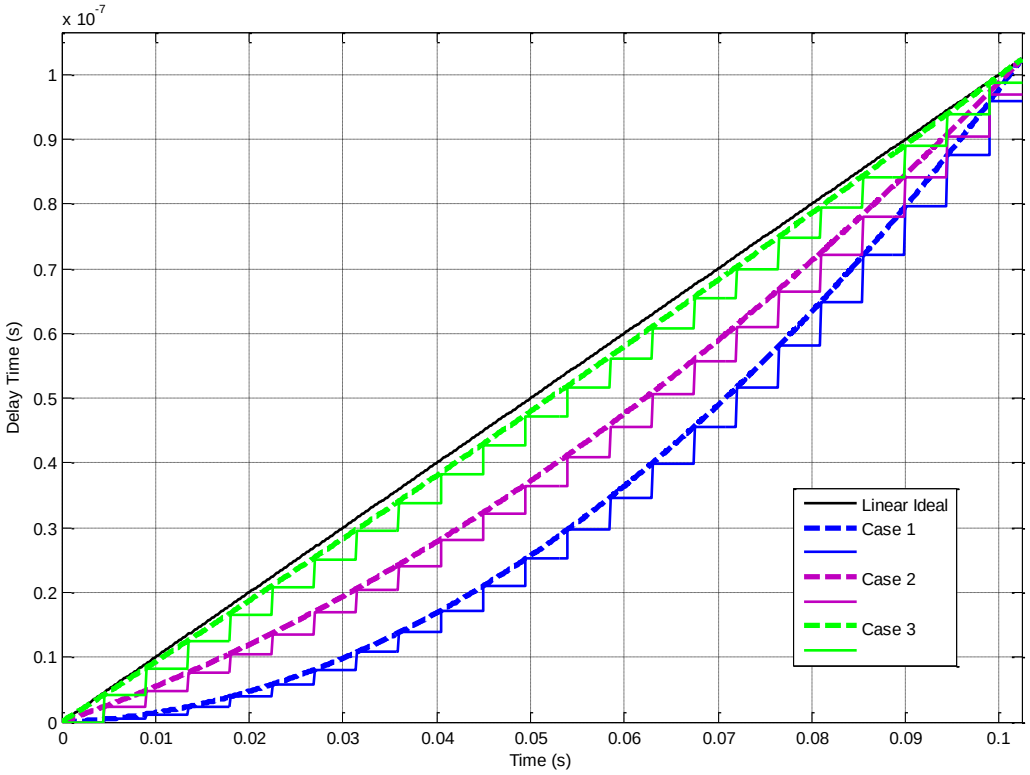

Figure 5.8 Discrete and real parabolic pull-off functions for case 1, 2 and 3

As shown in Table 5.3, in case 1, the DRFM parabolic RGPO function provides a very low separation from the real target echo in the first phase of the pull-off, then it separates false target with an accelerating movement. In case 2, parabolic RGPO function simulated with lower pull acceleration and higher pull-off rate to provide faster pull behavior. Finally, for case 3, RGPO function pull acceleration and pull-off rate parameters are selected as faster than then the case 2 and nearly linear pull function as shown Figure 5.8. In these three scenarios the false targets are pulled to same range with the linear case; in other words they give same time delay to false target signals with linear RGPO at the end of the CPI.

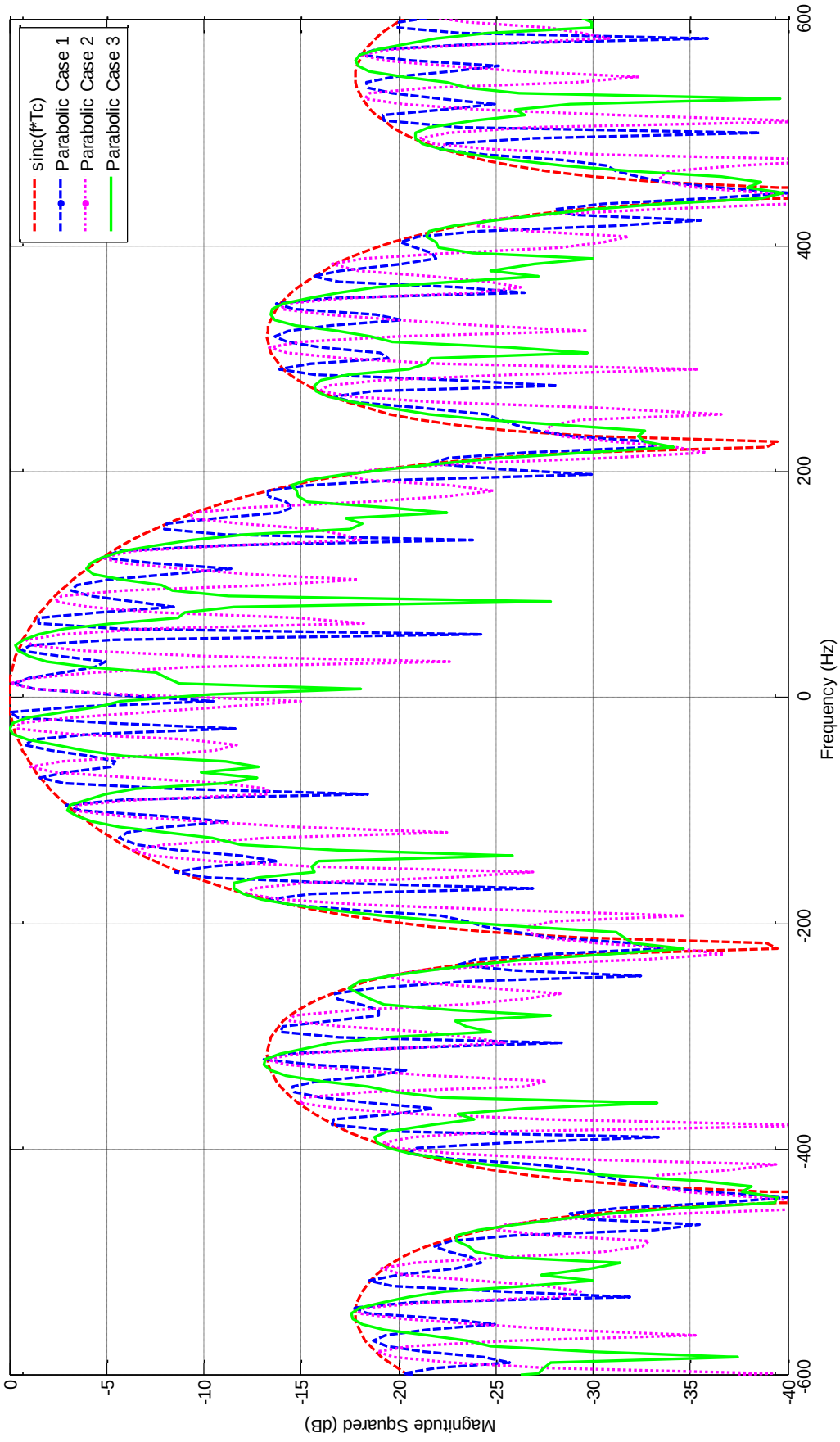

Figure 5.9 Discrete parabolic pull-off function spectrums for case 1, 2 and 3

Figure 5.9 shows the frequency spectrums of the parabolic RGPO signal according to the case 1, case 2 and case 3 parameters. Parabolic RGPO spectrum gives an oscillating wave under a *sinc* envelope. According to the equation (4.39) spectrum of the parabolic RGPO has a series of complex exponential, and its magnitude changes with a *sinc* whose bandwidth depends on the step length (T_c). In Figure 5.9, the *sinc* envelope, whose first null is 222.2 Hz, is shown in the spectrum for all cases since T_c parameter is used same as for these scenarios. As a result, the parabolic pull function fills the spectrum with the summation of complex exponential signal over a *sinc* function having a 444.4 Hz main lobe for these three parabolic RGPO spectrums. According to the first three scenarios, DRFM parabolic RGPO signal spectrum is a *sinc* function whose bandwidth changes with the step length (T_c) parameter. It is simply a summation of complex exponential signals. The changing factor for these spectrums is the oscillation density in the *sinc* envelope. Figure 5.9 shows that when pull function approaches to the linear function, its oscillating wave density decreases in *sinc* envelope, but it never turns into a linear RGPO spectrum. So, parabolic RGPO technique does not provide a specific spectrum to understand or get some clues about the applied EA technique by the side of signal intelligence.

Case 4 is a control scenario where DRFM parabolic RGPO function has a pull-off rate $\alpha = 1 \times 10^{-6}$ and pull acceleration $\varphi = 0$ in order to observe the RGPO spectrum behavior when there is no pull acceleration in the pull function. The scenario is applied by a parabolic pull function reducing the pull acceleration parameter to zero, and then applying a pull-off rate of the linear ideal function ($\alpha = 1 \times 10^{-6}$). Here, center frequency and CPI is fixed.

As shown in Figure 5.10, parabolic RGPO spectrum for this scenario turns into the linear RGPO spectrum. It has sequence of dirac deltas which are shifted from center by 31.75 Hz as in the linear RGPO case 1 since pull function has zero pull acceleration; in other words it has no quadratic component in its pull function that produces complex exponential series although its pull function is a parabolic form.

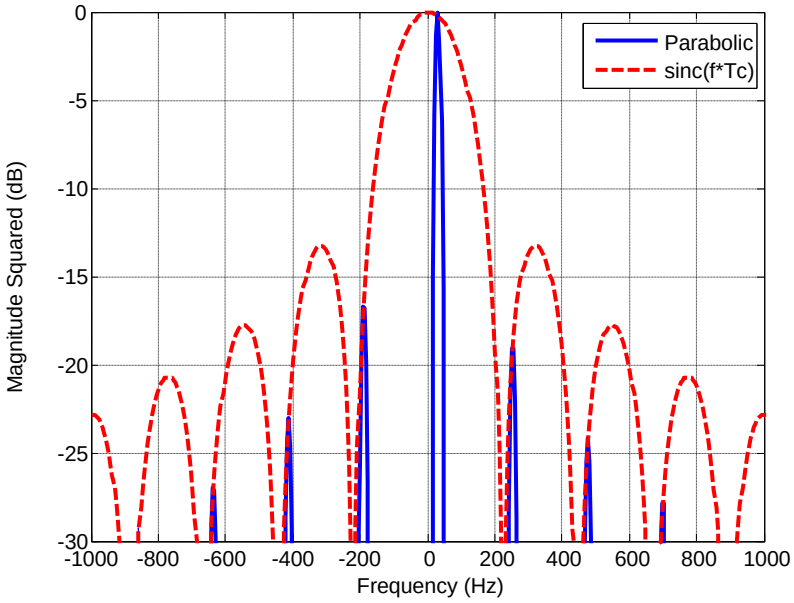

Figure 5.10 Discrete parabolic pull-off function spectrum for case 4

As final simulation, case 5 pull acceleration, pull-off rate, radar center frequency and CPI parameters are fixed as in case 1. The parameters that are varied are delay resolution and update period of DRFM for this scenario. In this scenario, parabolic RGPO technique is simulated with smaller delay resolution and update period ($t_d = 2.22$ ns $t_s = 0.75$) ms, hence they cause smaller step length parameter $T_c = 2.25$ ms according to the equation (3.35).

Spectrum of the applied parabolic RGPO signal is shown in Figure 5.11. As can be seen from the figure, parabolic RGPO spectrum gives an oscillating wave under a *sinc* envelope as expected. As explained in the previous scenarios, main lobe of the *sinc* depends on the step length (T_c). Hence, in this scenario, smaller t_d and t_s parameters causes a smaller T_c value. According to this parameter, first null of the *sinc* is expected as $1/T_c$ or 444.4 Hz. As a result, the parabolic pull function fills the spectrum with summation of the complex exponential signals explicitly on 888.8 Hz bandwidth *sinc* envelope.

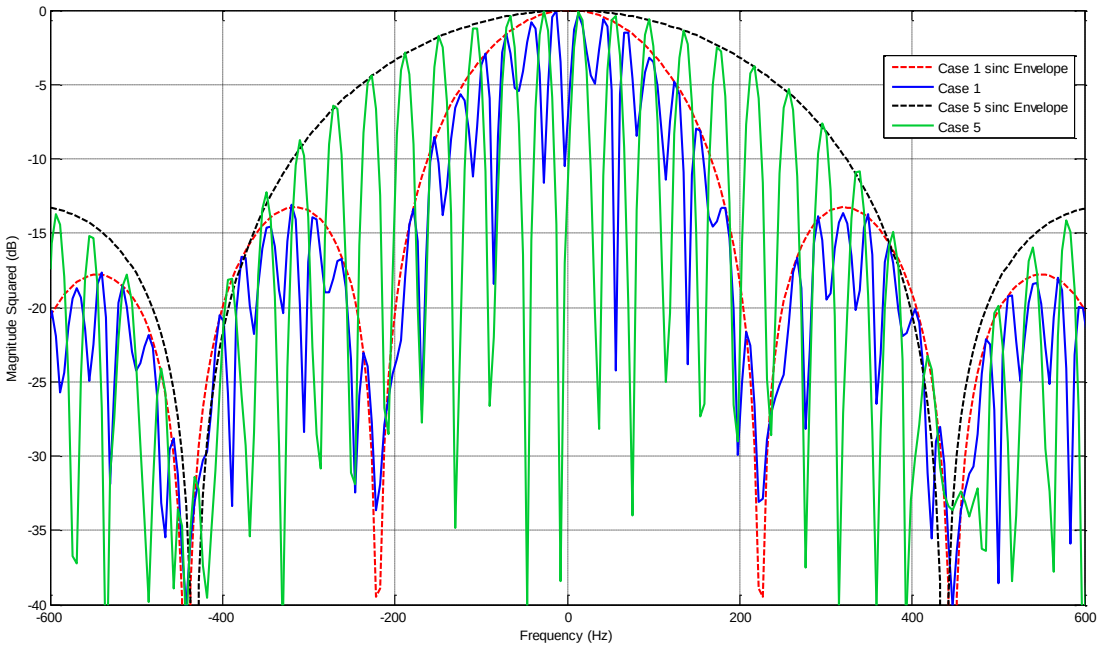

Figure 5.11 Discrete parabolic pull-off function spectrums for case 1 and 5

Finally, different CPI values are simulated to observe the effects of the CPI on DRFM parabolic RGPO technique. The parameters used in the simulation results are the same as case 1, except that two shorter CPIs are tried (25.6 ms and 12.8 ms) as in the linear RGPO section. Figure 5.12 shows the DRFM parabolic RGPO spectrums all together to compare effects of CPI values. Spectrum shows that the expected frequency oscillation is not visible at 12.8 ms CPI value, but visibility of the frequency oscillation improves when the CPI is chosen longer (25.6 ms and 102.4 ms). Hence, low CPIs do not show the details of the spectrum, so shorter CPI values may cause information losses in the spectrum.

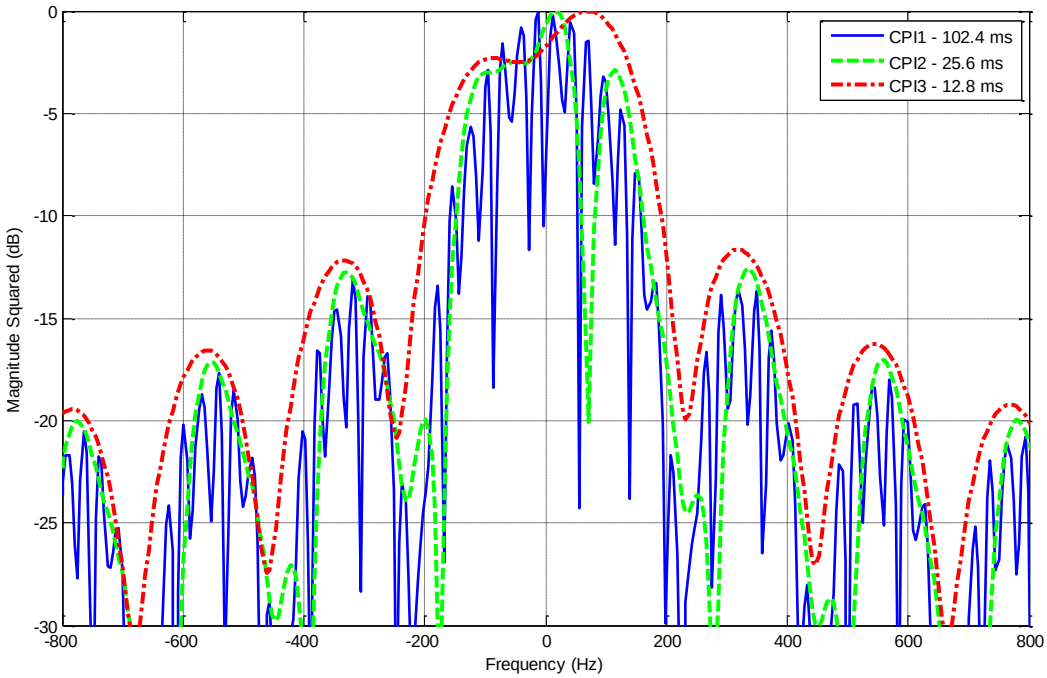

Figure 5.12 Discrete parabolic pull-off function spectrums for case 1 for all CPI values

CHAPTER 6

CONCLUSIONS

DRFM is a hardware which is used to generate false target echoes by memorizing and retransmitting the copied and changed target echo. It has an advantage with respect to the other repeater jammers since its ability to maintain coherency with the received radar signal. DRFM is a reliable platform to generate EA techniques like false target generation, RGPO, VGPO, etc. because of the capability of manipulating the copied radar signal in time, frequency and phase domains.

RGPO is one of the commonly used EA techniques with DRFM system to deceive hostile forces' radar systems in range domain. During RGPO operation, the copied radar signal by DRFM system is transmitted back to the target radar with a time delay with respect to the received radar signal. This time delay can be applied in a linear or parabolic (quadratic) fashion, and it is named as linear RGPO or parabolic RGPO according to the time delay (pull) function. Therefore, the gradually increasing time delay on the false target echo is understood in the target receiver as a walking away target in case the EA technique is successful.

In the literature previous researches have mainly focused on the spurious signals and harmonics which are occurred because of discrete behavior of the ADC unit of DRFMs. These studies provide results about the effects of the spurs and harmonics on DRFM signal, and reducing the spur effects with some methods. Also, some researches determine the quantization noise and phase performance of DRFMs. As different from these, in some studies discrimination of the DRFM RGPO signal and target pulse has investigated, and finally, DRFM linear RGPO signal, its spectral characteristics and magnitude of the harmonics are analyzed with limited number of researches.

In this thesis work firstly, EW and place of the DRFM in EW operations are explained with the previous studies about the DRFM as open literature survey. Then, a pulse Doppler radar signal which is used as input signal of the DRFM is derived with its time and frequency domain signal representations. Next, a DRFM system and its sub-blocks, also RGPO techniques which include linear and parabolic RGPO are explained in the same chapter. Also, RGPO technique is able to be applied as linear and parabolic according to the pull function is derived with analytical expressions under linear RGPO and parabolic RGPO sections. In these sections pull functions is applied to the DRFM input signal as a delay function is expressed and spectrums of these pull functions are obtained. Finally, results of the computer simulations for different linear and parabolic RGPO scenarios are given to verify the validity of analytical derivations.

In the linear RGPO simulations a small center frequency shift is observed in the spectrum because of the discrete behavior of the DRFM. The linear RGPO signal spectrum is formed multiplication of a *sinc* function and summation of the dirac delta functions. From linear RGPO signal derivations a result is observed that the total frequency shift of the dirac delta sequence depends on the step size (delay resolution), step length and radar center frequency. In the case of step size and radar center frequency multiplication is a fractional number, center frequency shifts and harmonics appear in the spectrum. Hence, size of the frequency shift, and magnitudes and location of the harmonics depend on the DRFM hardware parameters, RGPO technique parameters and also radar parameters of the target. Five linear RGPO scenarios are considered to observe the linear RGPO signal spectrum when pull-off rate, DRFM parameters (delay resolution (t_d) and update period (t_s)) and radar frequency are changed. As a result of these simulations, according to the used parameter set the center frequency shift can be a few ten Hz or a few hundred Hz, or it can result in zero center frequency shift with the appropriate parameters.

The other simulations are realized for DRFM parabolic RGPO technique. Five parabolic RGPO scenarios are simulated to observe the spectrum when pull function and DRFM parameters (delay resolution (t_d) and update period (t_s)) are changed. In these simulations an oscillatory exponential signal with a *sinc* envelope is obtained differently from linear RGPO. This has an expected result according to the analytical

derivations, since the spectrum of the DRFM parabolic RGPO signal is formed multiplication of a *sinc* function, which is bandwidth is related with the step length (T_c) of the DRFM, and summation of complex exponential functions. In the simulations the oscillating wave density changing is observed according to the pull function however the center frequency does not change.

Finally, in the EA side of DRFM linear RGPO technique, the parameters should be chosen according the target radar parameters and it is specified such that it causes minimum frequency shift insofar as hardware limit permits; on the other hand, the technique parameters or hardware limits can be identified according to the occurred center frequency shift and spectral lines when looking from the signal intelligence side. Otherwise, DRFM parabolic RGPO technique does not provide so much clues about the EA technique since it has no frequency shift or magnitude changing in the spectrum except that the oscillation density and bandwidth of the *sinc* envelope. So, parabolic RGPO technique is more powerful than linear RGPO in EA side however in signal intelligence side additional studies may be helpful to find out the EA technique properties.

For the future works, the linear RGPO signal spectrum can be analyzed for real, especially air-to-air, engagement scenarios by adding the Doppler effect to examine center frequency shift in the spectrum. Furthermore, additional methods can be discussed to eliminate the center frequency shift to improve the linear RGPO technique. Also, to evolve the parabolic RGPO technique the signal suppression methods can be analyzed to reduce signal oscillation in the parabolic RGPO signal spectrum. Moreover, supplementary simulations can be performed by using the real DRFM hardware parameters to show the spectrum results for both linear and parabolic RGPO techniques. Finally, supplementary studies can be done to extend the analysis to provide how the discrete nature of the DRFM effects other EA techniques which are using generally with RGPO technique such as VGPO.

REFERENCES

[1] Schleher, D. C., (1986), *Introduction to Electronic Warfare*, Artech House

[2] Joint Publication 3-13.1 Electronic Warfare, 25 January 2007

[3] Neri, F., (2001), *Introduction to Electronic Defense Systems*, Artech House

[4] Dinç V., (2010), Elektronik Harp Teknikleri, Gazi University Institute of Science and Technology

[5] Singh M., (1988), *Electronic Warfare*, Defence Scientific Information & Documentation Centre (DESIDOC) Ministry of Defence, DRDO

[6] Berger, S. and Meer, D. E., (1990), An expression for the frequency spectrum of a digital radio frequency memory signal. In Proceedings of the IEEE 1990 National Aerospace and Electronics Conference, 90-93.

[7] Roome, S., (1990), Digital radio frequency memory. Electronic and Communication Engineering Journal, 2 (Aug. 1990), 147-153.

[8] Kernis, W., (1991), Spur levels in multiple-bit DRFMs. Journal of Electronic Defense, (Jan. 1991), 49-54.

[9] Gold, D., and Ur, H., (1993), Method for reduction of harmonics, caused by coarse quantisation, suitable for digital radio frequency memory. Electronics Letter, 411-412.

[10] Hill, P. C., and Truffert, V., (1992), Statistical processing techniques for detecting DRFM repeat-jam radar signals. In IEE Colloquium on Signal Processing Techniques for Electronic Warfare, 1992, 1/1-1/6.

[11] Dunn-Rogers, J., (1991), An analysis of the performance of DRFMs for EW systems. In IEE Colloquium on Electronic Warfare Systems, 1991, 2/1-2/4.

[12] Pring, P., James, G., Hayes, D., and White, M., (1994), The phase performance of the digital radio frequency memories (DRFMs). In Second International Conference on Advanced A-D and D-A Conversion Techniques and their Applications, 1994, 18-23.

[13] Blair, W., and Brandt-Pearce, M., (1997), Discrimination of targets and RGPO echoes using frequency diversity. In Proceedings of the Twenty-Ninth Southeastern Symposium on Systems Theory, 1997, 509-513.

[14] Berger, S. D., (2001), The spectrum of a digital radio frequency memory linear range gate stealer electronic attack signal. In Proceedings of the 2001 IEEE Radar Conference, Atlanta, GA, May 2001, 27-30.

[15] Berger, S. D., (2003), Digital Radio Frequency Memory Range Gate Stealer Spectrum. IEEE Transactions on Aerospace and Electronic Systems, vol. 39, No:2.

[16] Bandiera, F., Farina, A., Orlando, D. and Ricci, G., (2010), Detection Algorithms to Discriminate Between Radar Targets and ECM Signals. IEEE Transactions on Signal Processing, vol. 58, No. 12.

[17] Olivier, K., Cilliers, J.E. and Plessis, M.du, (2011), Design and performance of wideband DRFM for radar test and evaluation. Electronics Letters, vol. 47 No. 14.

[18] Sward, W. S. and Reed, D. E., (2010), Phase Continuous Radar Test Set. AUTOTESTCON, 2010 IEEE, pp.1-5.

[19] Skolnik, M. I., (2008), *Radar Handbook*, McGraw Hill

[20] Skolnik, M. I., (1980) *Introduction to Radar Systems*, McGraw-Hill

[21] Stimson G.W., (1998), *Introduction to Airborne Radar*, SciTech Publishing

[22] Scorpion 2 RECM, http://www.thalesgroup.com, Accessed January, 2015

[23] NAVAIR Electronic Warfare/Combat Systems, "*Electronic Warfare and Radar Systems Engineering Handbook"*, 1 April 1997

[24] Richards, M. A., (2005), *Fundamentals of Radar Signal Processing*, McGraw-Hill

APPENDIX

- **Linear Case 1**

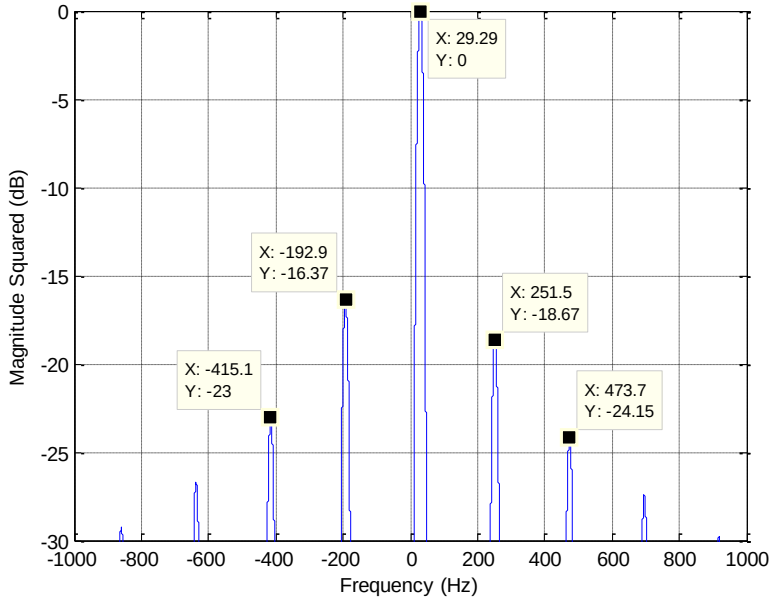

Figure A.1 Linear RGPO case 1

- **Linear Case 2**

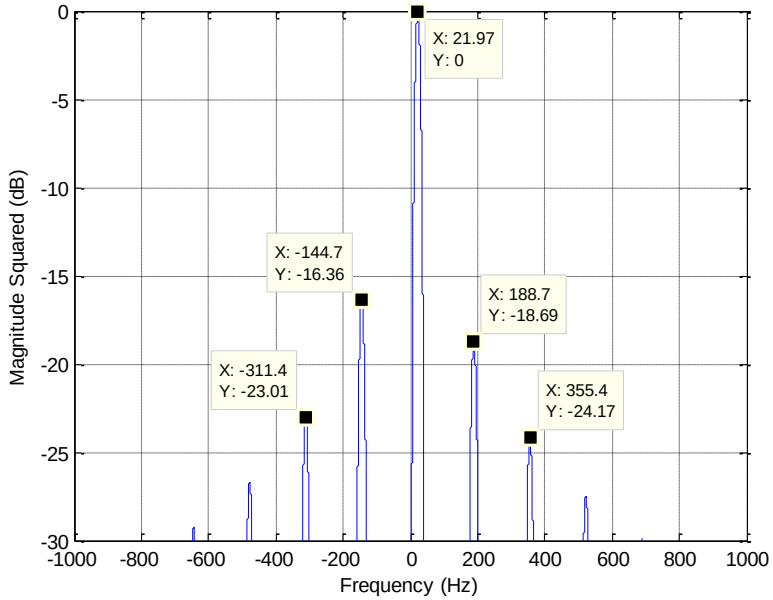

Figure A.2 Linear RGPO case 2

- **Linear Case 3**

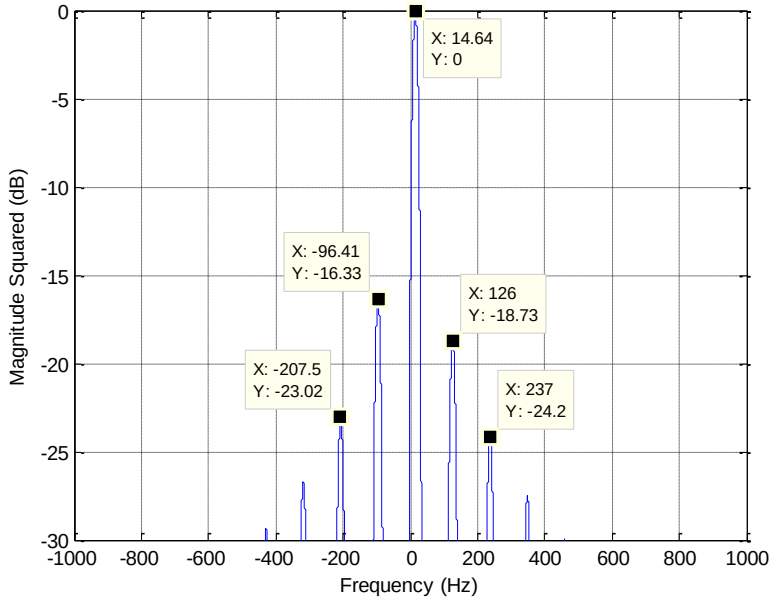

Figure A.3 Linear RGPO case 3

- **Linear Case 4**

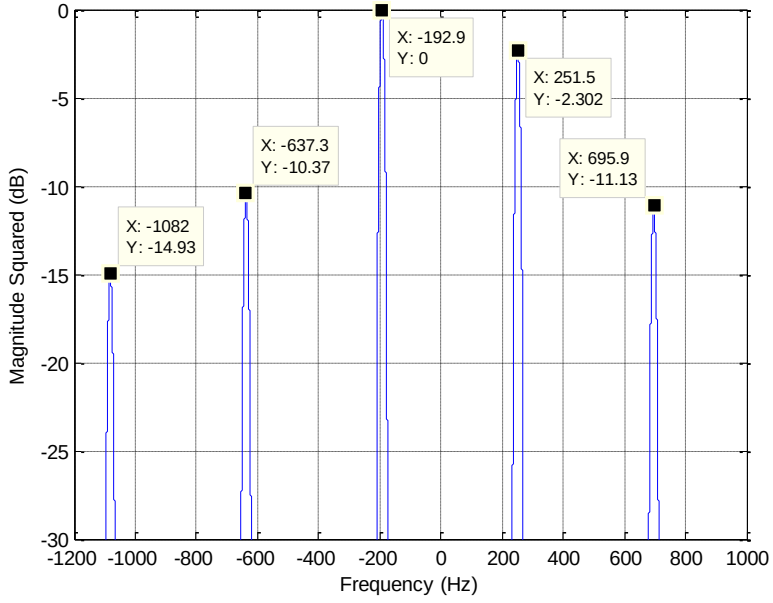

Figure A.4 Linear RGPO case 4